Molecular-Dynamics Studies of Single-Stranded Hexitol, Altritol, Mannitol, and Ribose Nucleic Acids (HNA, MNA, ANA, and RNA, Resp.) and of the Stability of HNA · RNA, ANA · RNA, and MNA · RNA Duplexes

by **Mattheus Froeyen**, **Berthold Wroblowski**, **Robert Esnouf**, **Hans De Winter**, **Brigitte Allart**, **Eveline Lescrinier**, and **Piet Herdewijn***[1])

Rega Institute for Medical Research, K. U. Leuven, Minderbroedersstraat 10, B-3000 Leuven

Dedicated to Professor *Albert Eschenmoser* on the occasion of his 75th birthday

The influence of the orientation of a 3′-OH group on the conformation and stability of hexitol oligonucleotides in complexes with RNA and as single strands in aqueous solution was investigated by molecular-dynamics (MD) simulations with AMBER 4.1. The particle mesh *Ewald* (PME) method was used for the treatment of long-range electrostatic interactions. An equatorial orientation of the 3′-OH group in the single-stranded D-mannitol nucleic acid (MNA) m(GCGTAGCG) and in the complex with the RNA r(CGCAUCGC) has an unfavorable influence on the helical stability. Frequent H-bonds between the 3′-OH group and the O–C(6′) of the phosphate backbone of the following nucleotide explain the distorted conformation of the MNA · RNA complex as well as that of the single MNA strand. This is consistent with experimental results that show lowered hybridization potentials for MNA · RNA complexes.

An axial orientation of the 3′-OH group in the D-altritol nucleic acid (ANA) a(GCGTAGCG) leads to a stable complex with the complementary RNA r(CGCAUCGC), as well as to a more highly preorganized single-stranded ANA chain. The averaged conformation of the ANA · RNA complex is similar to that of A-RNA, with only minor changes in groove width, helical curvature, and H-bonding pattern. The relative stabilities of ANA · RNA *vs.* HNA · RNA (HNA = D-hexitol nucleic acid without 3′-OH group) can be explained by differences in restricted movements, H-bonds, and solvation effects.

1. Introduction. – Realistic molecular-dynamics (MD) simulations of nucleic acids have been difficult to perform because of the poor treatment of the highly charged phosphates in the force fields. They failed to reproduce stable conformations close to experimentally defined X-ray or NMR structures. Recent developments in the treatment of long-range charge interactions, like the particle mesh *Ewald* (PME) method [1], allow computations of highly charged systems without an explosion in computational effort [2][3]. MD Simulations of natural RNA and DNA complexes can now be performed on average structures close to the experimentally determined ones [4–6]. These results encouraged us to perform MD simulations of sugar-modified nucleic acids for which no structures are known, to give us a first insight into their structural features.

D-Hexitol nucleic acids (HNAs), *i.e.*, nucleic acids with 1′,5′-anhydro-2′,3′-didehydro sugar moieties, are new oligomeric structures that are able to hybridize sequence-selectively both with themselves and with natural nucleic acids [7–9]. They are able to support an efficient information transfer in nonenzymatic template-directed reactions [10][11] and are highly enantioselective [12]. The introduction of an OH group at the

[1]) Phone: +32-16-337387; fax: +32-16-337340; e-mail: Piet.Herdewijn@rega.kuleuven.ac.be.

3′-position of HNA alters the hybridization properties considerably (*Fig. 1*). When the OH group is introduced in the 3′β position ((3′*R*)-configuration), D-mannitol nucleic acids (MNAs) are obtained [13]. However, MNAs form duplexes with RNA of low stability. When the OH group is introduced in the 3′α position ((3′*S*)-configuration), D-altritol nucleic acids (ANAs) are obtained [14]. These nucleic acids hybridize strongly and sequence-selectively with RNA in an antiparallel way. The order of stability as derived from the melting temperatures of the duplexes is ANA · RNA > HNA · RNA > RNA · RNA > MNA · RNA for the sequence a-, h-, r-, and m(GCGTAGCG) · r(CGCAUCGC) [15]. To understand the influence of the 3′-OH group on duplex stability, the conformations of the different single-stranded and double-stranded nucleic acids were investigated by molecular modeling and free MD simulations in aqueous solution. The modeling studies on the HNA · RNA reference have been described previously [6].

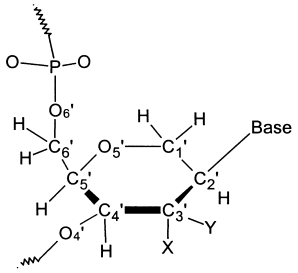

HNA X = H, Y = H

ANA X = OH, Y = H

MNA X = H, Y = OH

Fig. 1. *Sugar moiety of HNA, ANA, and MNA*

2. Materials and Methods. – *Force-Field Parameters and Partial Charges.* The force-field parameters and partial charges for RNA were taken from the AMBER 4.1 force field parameter database [16]. The force-field parameters for ANA and MNA were taken from AMBER 4.1 without modification. The partial charges of ANA and MNA were obtained by a two-stage fitting procedure (RESP [17]) from the 6-31G*-derived electrostatic potential calculated with GAMESS (version May 1995) [18]. The partial atomic charges and force field atom types of the ANA and MNA residues are shown in *Fig. 2*.

Model Building. Model building was performed with the AMBER 4.1 software [16] and tools. For visualization, Rasmol [19] and MidasPlus [20] were used. The modeling of the ANA · RNA complex in A-RNA geometry was done by modeling d(GCGTAGCG) · r(GCGUACGC) (d and r = D-2′-deoxyribose and D-ribose moiety, resp.) in *Arnott*'s canonical A-RNA geometry [21] and subsequent fitting of the a(GCGTAGCG) (a = D-altritol moiety) strand onto the DNA strand. The ANA strand was then minimized by restraining the base atoms to the corresponding positions of the DNA strand with a force constant of 10 kcal/mol Å^2 per atom. After deletion of the DNA strand, the ANA · RNA complex was energy-minimized to an r.m.s. gradient of 0.1 kcal/mol Å using restraints on the base H-bonds (10 kcal/mol Å^2). The resulting duplex was put in a rectangular box of TIP3P water [22] extending approximately 12 Å in each direction from the nucleic-acid atoms. The 14 H_2O molecules with the most negative electrostatic potentials were replaced by Na^+ ions, leaving 3529 H_2O molecules in an initial box of $50.9 \times 43.7 \times 45.9$ Å^3. For the single-stranded starting model, single-strand ANA was taken from the duplex ANA · RNA and placed in a H_2O box, and the 7 H_2O molecules with the most negative electrostatic potential were replaced by Na^+ ions, resulting in a rectangular box of $50.0 \times 40.6 \times 36.3$ Å^3

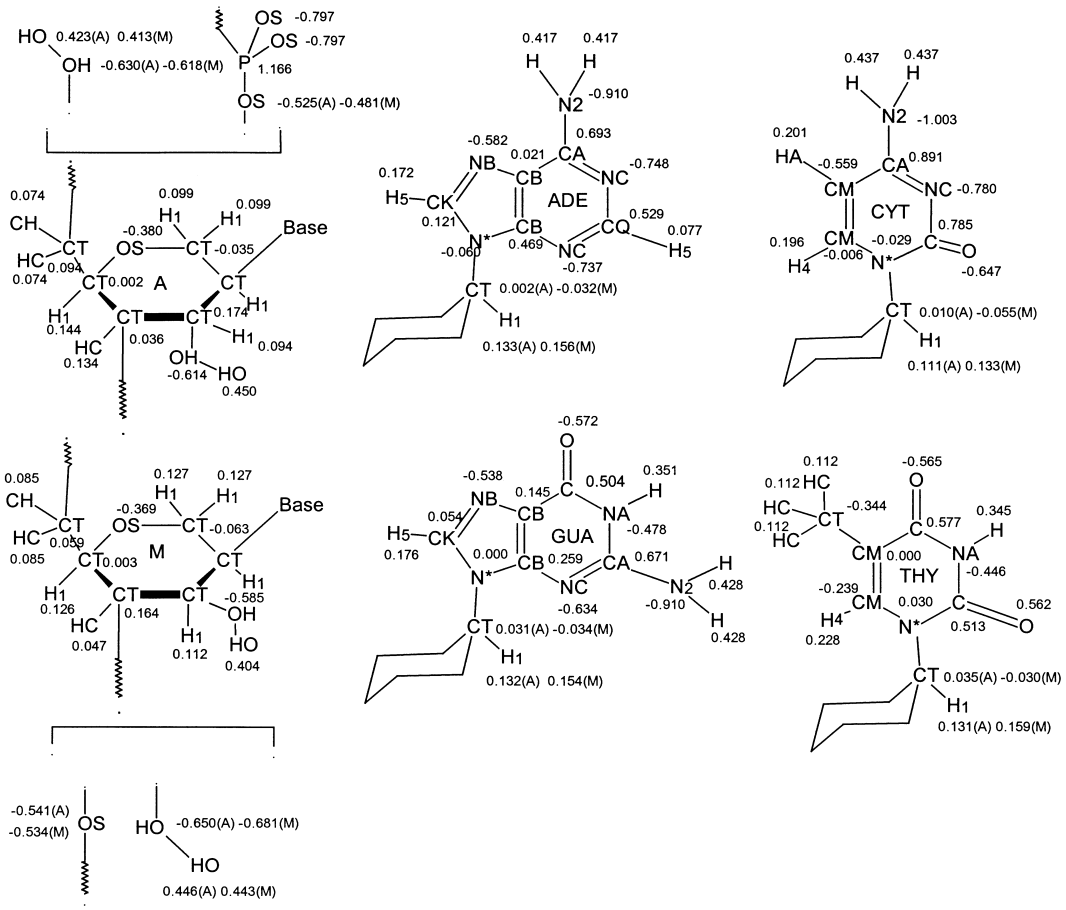

Fig. 2. *Force-field atom types and partial charges for the different nucleotides*

with 2347 H_2O molecules. The same procedure was followed when creating the MNA · RNA, the single-stranded MNA, and the equivalent HNA and RNA systems.

Molecular-Dynamics Simulations. The MD-simulation parameters are summarized in *Table 1*. The simulations were at constant temperature (300 K) with separate-but-equal temperature coupling time constants of 0.4 ps^{-1} for solute and solvent atoms, and at constant pressure (1 bar) with a compressibility of $44.6 \cdot 10^{-6}$ bar^{-1} and a pressure relaxation time of 0.4 ps^{-1} [23]. The integration time step was 2 fs, and SHAKE [24] was applied to all bond lengths. A 9-Å cutoff was used for the *Lennard-Jones* interactions with the non-bonded pair-list updated every 10 steps. Long-range electrostatic interactions were treated by the particle mesh *Ewald* (PME) method [1] with a PME charge-grid spacing of *ca.* 1 Å in each direction, an order of 4 for the β spline interpolation, and a direct sum tolerance of 10^{-4}. Equilibrium was achieved by energy minimization of the whole system until the gradient of the energy dropped below 0.1 kcal/mol Å. The systems were heated to 300 K within 10 ps, after which the production runs over 1 ns for the duplexes ANA · RNA and MNA · RNA and the single-stranded (ss) ANA, MNA, HNA, and RNA were initiated. Conformations were saved every 0.2 ps. The energy minimizations and the MD simulations were performed with the SANDER module of AMBER 4.1 [16].

MD Trajectory Analysis. Potential-energy values were extracted from the SANDER output files. The following properties were extracted from the MD trajectories by the CARNAL module of AMBER 4.1 [16]: H-bonding patterns, distances between atoms, root-mean-square deviations from the starting conformation, and torsion angles. The cutoff distance between the heavy H-bond donor and acceptor atoms was 3.3 Å, and the cut-

Table 1. *Simulation Conditions and Parameters*

	ANA · RNA	MNA · RNA	ssANA	ssMNA [a])	ssHNA [a])	ssRNA [a])
Total number of atoms	11331	11331	7335	7335	7702	7398
Number of solute atoms	541	541	287	287	279	254
Number of Na^+ counterions	14	14	7	7	7	7
Number of TIP3P H_2O molecules	3592	3592	2347	2347	2472	2379
Total simulation time [ps]	1000	1000	1000	1000	1000	1000
Initial box dimensions [Å]						
x	51	51	50	50	50	50
y	44	44	41	41	41	41
z	46	46	36	36	36	36
Equilibration time [ps]	10	10	10	10	10	10
Thermodynamic ensemble	(N, P, T)					
Integration algorithm	Verlet					
Constraints	SHAKE for bond lengths					
Integration timestep [ps]	0.002					
Temperature regulation	heat bath					
Time constant [ps^{-1}]	0.4					
Reference temperature [K]	300					
Pressure regulation	isotropic position scaling					
Pressure relaxation time [ps^{-1}]	0.4					
Reference pressure [bar]	1					
Vdw interactions cutoff [Å]	9					
Relative electrostatic dielectric constant	1					
Electrostatics calculation method	PME (particle mesh *Ewald*)					
Software	AMBER 4.1					

[a]) ss = single-stranded.

off H-donor-acceptor angle was 45° (0° is linear). The sugar-puckering parameters for the hexitol sugars were calculated according to *Cremer* and *Pople* [25], and the parameters for the ribose sugars were calculated according to *Altona* and *Sundaralingam* [26]. The radial distribution functions g(r), which gives the probability of finding an atom at a distance r from another atom, were calculated for the 3′-OH groups with a small custom program.

Solvent-Accessible Surface Areas. Solvent-accessible surfaces were calculated with the d.m.s. program in the MidasPlus package [20] which follows the definition by *Richards* [27]. The solvent probe radius was 1.4 Å and the *van der Waals* radii of C-, O-, N-, and P-atoms were 1.9, 1.4, 1.5, and 1.9 Å, respectively. All H-atoms were removed from the structures before calculation.

Nucleic-Acid Double-Helix Curvature. The curvature of the double helices was examined using a version of the Curves 5.0 program [28] modified to take into account the different topology of hexitol sugars.

Torsion Driving. To investigate the flexibility of the ANA, MNA, and HNA backbones and the interactions of the 3′-OH groups with these backbones, torsion maps were calculated. One series of maps shows energy as a function of the torsion angles α and ζ, and another series shows energy as a function of the torsion angles ε and ζ, both series calculated for the dinucleotides G_hpC_h, G_apC_a, and G_mpC_m with the 3 different sugar moieties D-hexitol (h), D-altritol (a), and D-mannitol (m). See *Fig. 3* for the definition of these torsion angles. These calculations were carried out in vacuum, with the same AMBER 4.1 force field and atom charges as in the MD simulations except that the dielectric was made distance dependent. The torsion angles γ, β, and ε were kept constant at 81, 167, and 212°, resp., during the calculation of the α,ζ maps. In the ε,ζ maps, the values of α, γ, and β were fixed at 281, 81, and 167°. These values are close to the equilibrium values for the HNA and ANA strands in the HNA · RNA and ANA · RNA MD simulations.

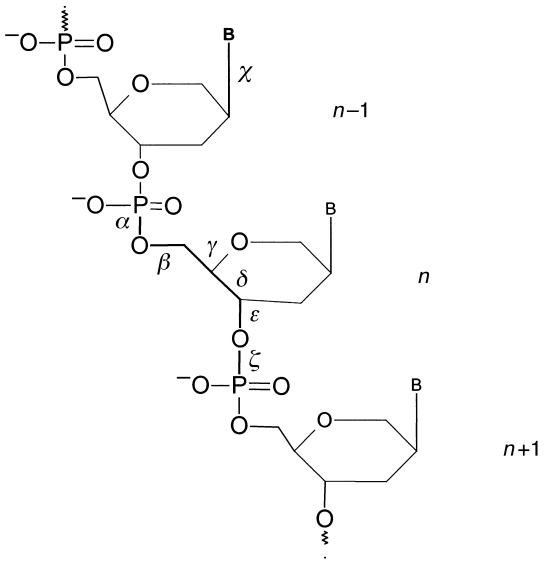

Fig. 3. *Definitions of the torsion angles in the polynucleotides*

Sample Preparation. The RNA strand r(CGCUACGC) was purchased from *Eurogentec*. Synthesis of the HNA molecule h(GCGTAGCG) and ANA molecule a(GCGUAGCG) was performed by means of phosphoramidite chemistry as described before [8][14]. The HNA and ANA phorphoramidite building blocks were synthesized as described previously [29][30].

Both oligonucleotide strands were dissolved in H_2O/D_2O 9:1, and the pH was adjusted to 7. The RNA soln. was titrated with an ANA soln. to obtain an mixture with a small excess of RNA. A soln. of 2.17 mg of RNA (1.125 nmol, pH 7.0) in 0.400 ml of D_2O was used as a starting point. After adding each aliquot of the ANA soln., the mixture was briefly heated to 80° and slowly cooled to r.t. to promote duplex formation. The degree of complex formation was monitored by 1D ^{1}H-NMR. After reaching the RNA/HNA 1.05:1 titration point, the sample was lyophilized and dissolved in 0.75 ml of D_2O to yield a 1.0 mM duplex soln.

NMR Spectroscopy. Varian-500-unity spectrometer operating at 499.505 MHz, quadrature detection by the *States-Haberkorn* hypercomplex mode [31]; spectra processing by *Varian* VNMR software; δ(H) rel. to internal acetate (=1.92 ppm) [31], δ(P) rel. to external trimethyl phosphate (=0 ppm); 1D spectra (H_2O) were recorded by means of a jump-return observation pulse [32]. NOESY [33] Experiments (D_2O): 5000-MHz sweep width in both dimensions, at 20 and 50° with mixing times 50 and 150 ms, resp., 32 scans, 2048 data points in t_2 and 512 increments in t_1. ^{1}H,^{31}P-HETCOR Experiments [34]: at 20 and 50° with 128 scans, 2048 data points in the ^{1}H-dimension t_2 and 512 real data points in the ^{31}P-dimension t_1, over sweep widths of 5000 and 2000 Hz, resp.; data apodization with a shifted-sine-bell square function in both dimensions and processing to a $2K \times 1K$ matrix.

3. Results. – 3.1. *Total Potential Energy. Fig. 4* shows the total potential energy E_p during the MD simulations. The ANA · RNA system is clearly more stable than the MNA · RNA system (*Fig. 4,a*). The energies can be compared because the systems are isomeric, having the same numbers and kinds of atoms. Likewise, the single-stranded ANA shows a greater stability than the MNA system (*Fig. 4,b*).

3.2. *Root-Mean-Square* (r.m.s.) *Deviations. Double-Stranded Simulations.* The r.m.s. deviations of all nucleic-acid atoms during the time course of the double-stranded simulations (*Fig. 5,a*) shows that the HNA · RNA and ANA · RNA result in similar deviations from the starting A-form double helix. In the case of the ANA · RNA

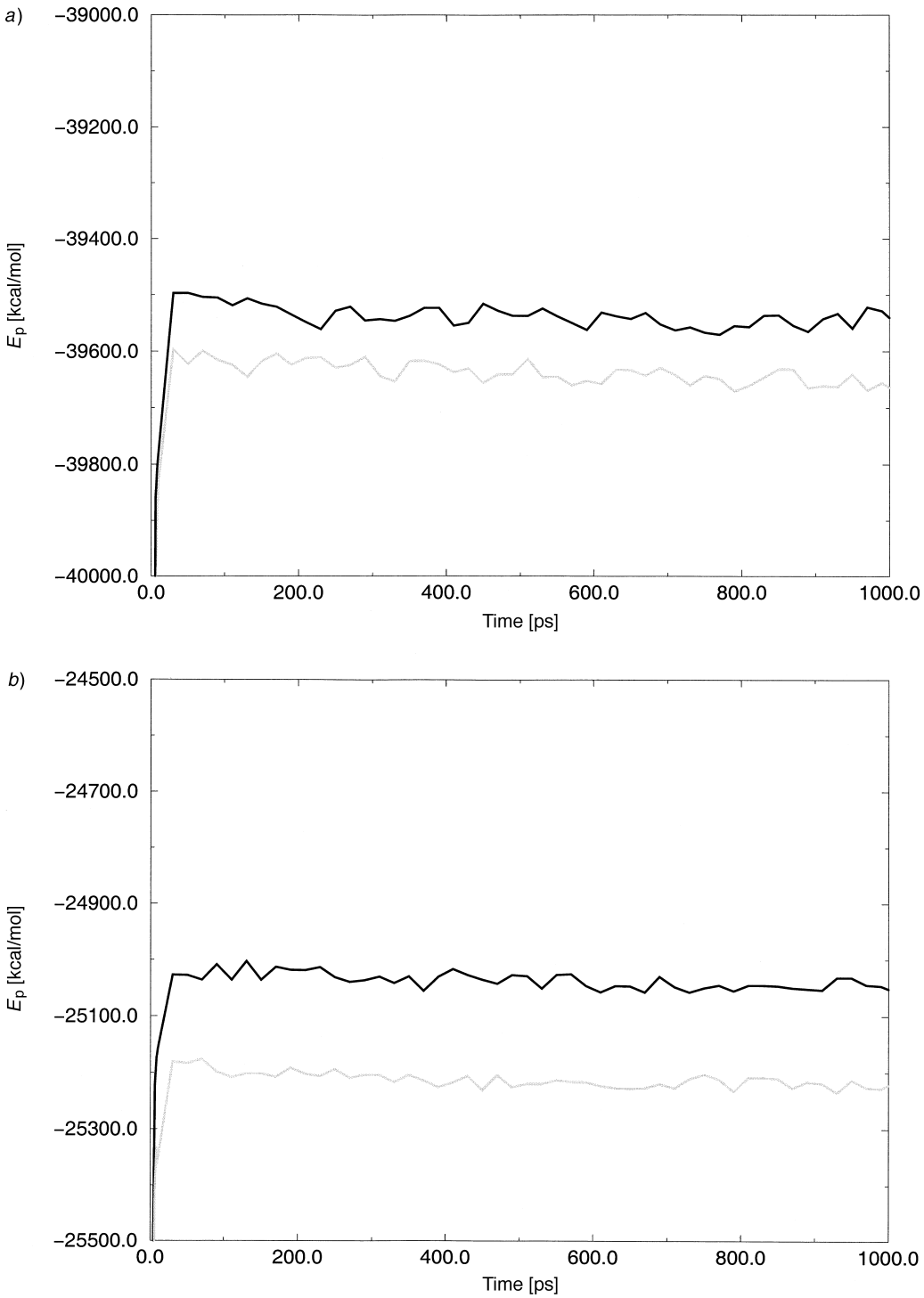

Fig. 4. *Total potential energy* (E_p) *during MD simulation for* a) *the double-stranded complexes MNA · RNA* (black) *and ANA · RNA* (gray), *and* b) *the single-stranded nucleic acids MNA* (black) *and ANA* (gray)

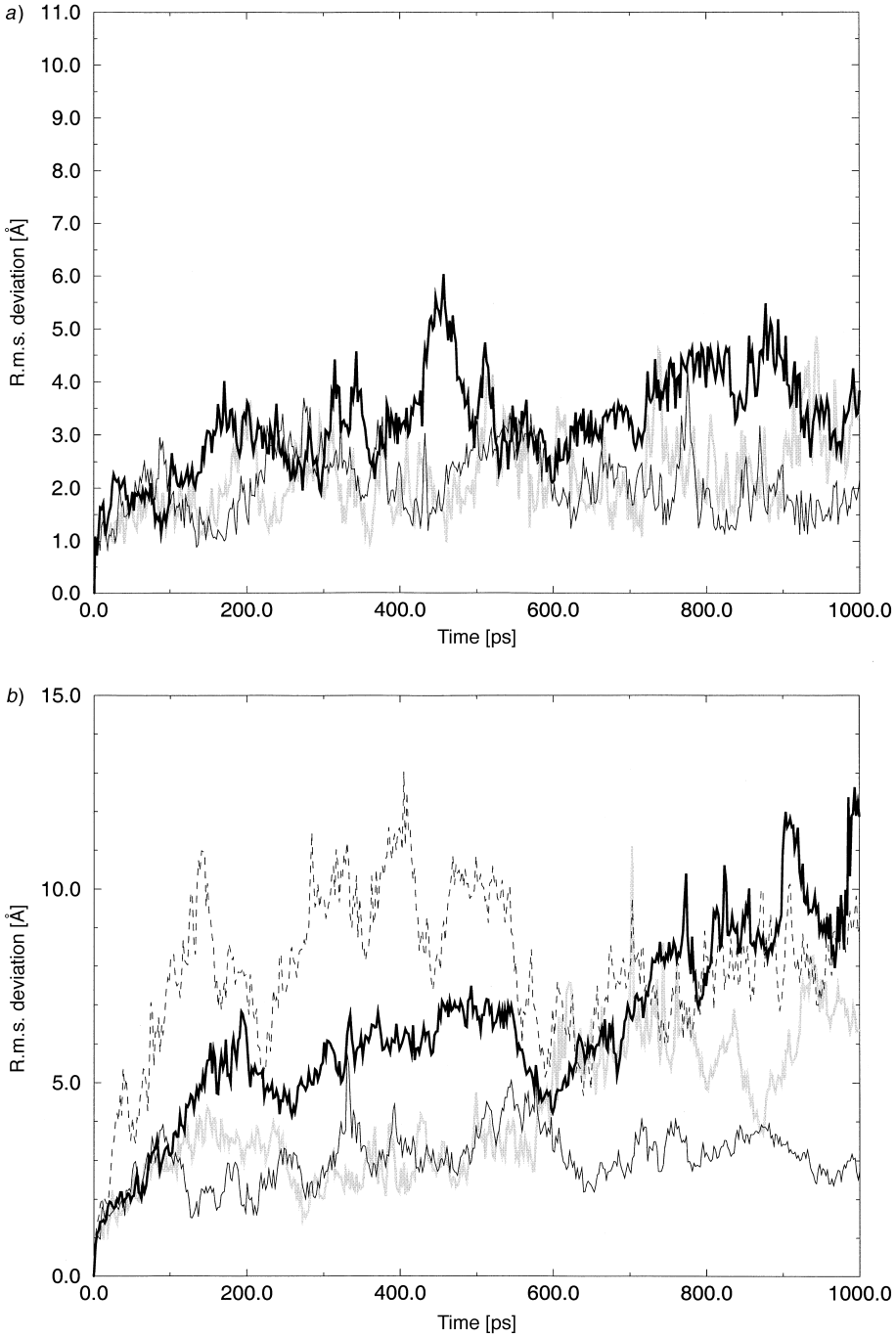

Fig. 5. *Root-mean-square* (r.m.s.) *atomic deviations of the nucleic-acid structures during the course of the simulations:* a) *Deviations for the double-stranded structures MNA·RNA* (black), *ANA·RNA* (gray), *and HNA·RNA* (thin black) (for the final 200 ps of the simulations, the mean r.m.s. deviations were 3.6 Å (MNA·RNA), 2.4 Å (ANA·RNA), and 2.2 Å (HNA·RNA). b) *Deviations for the single-stranded structures MNA* (black), *ANA* (gray), *HNA* (thin black), *and RNA* (dashed).

complex, deviations are on average less than 3 Å from the starting conformation. The MNA · RNA structure on average shows somewhat greater deviations from the starting structure.

Single-Stranded Simulations. The r.m.s. deviations of the single-stranded simulations (*Fig. 5,b*) show that single-stranded RNA (ssRNA) deviates most from the starting A-form conformation and seems to be very flexible. ssHNA and ssANA both stay close to the starting A-form structures, up to 600 ps, where ssANA starts to deviate from it. ssMNA seems to unwind shortly after the start of the simulation, but more slowly than ssRNA. This different behavior of the MNA chain is also observed in the double-stranded simulations where the r.m.s. deviation of MNA · RNA is larger than those of ANA · RNA and HNA · RNA. The presence of the 3′-OH group and the configuration at C(3′) is determining for this effect. The 3′β orientation of the OH group destabilizes the A-form conformation as seen in ssMNA. In contrast, ssHNA and ssANA (with a 3′α orientation of the OH group) have a more stable conformation.

3.3. *Molecular Structures. Snapshots During the Single-Stranded Simulations. Fig. 6,a* shows snapshots of ANA, HNA, MNA, and RNA single-stranded structures. ANA and HNA have remained close to the starting A-form conformations, but at 600 ps, single-stranded ANA starts to unfold. Single-stranded MNA partially unwinds during the simulation, forming a kink at the position of the pT_mpA_m in the center of the strand. Single-stranded RNA totally unwinds, without any remaining intramolecular H-bonds or base-stacking interactions. This confirms the picture of free unhindered movements in RNA but restricted movements in the HNA, ANA, and MNA chains.

Average Structures of Double-Stranded Nucleic Acids. Fig. 6,b shows the averaged ANA · RNA and MNA · RNA double-stranded structures. The ANA · RNA structure is still in the A-form conformation. MNA · RNA exhibits a large conformational change, drifting away from its starting conformation. The shape of the MNA · RNA duplex resembles the conformation of ssMNA. As ssMNA is more preorganized than ssRNA, we hypothesize that the MNA chain is the cause of this rearrangement, with the more flexible RNA strand fitting to the preferred MNA conformation.

3.4. *Curvature of the Double Helices.* The helical axis, computed by the Curves program [28], is nearly straight in ANA · RNA (*Fig. 7,c*), with a small kink at the central T4 · A13 pair but with the average head-to-tail distance about the same as in double-stranded RNA (19.59 Å *vs.* 19.67 Å) (*Fig. 7,a*). HNA · RNA (*Fig. 7,b*) shows the same kink at residue pair $T_h4 \cdot A_h13$. The average head-to-tail distance of the double helix is somewhat larger at 20.9 Å. In MNA · RNA (*Fig. 7,d*), the helical axis becomes more curved and the head-to-tail distance drops to 16.1 Å.

3.5. *Base-Pair Hydrogen Bonds and Minor-Groove Width.* In *Table 2*, a summary of the base-pair H-bond lengths for the complexes ANA · RNA and MNA · RNA is given. Note the high standard deviations in the MNA · RNA simulation. The base-pair H-bonds, especially those facing the major groove, are weaker in MNA · RNA than in ANA · RNA (or HNA · RNA [6]), but not completely broken. This is most pronounced in the central A5 · U12, T4 · A13, and G3 · C14 pairs, where the distances can reach up to 4.3 Å. The conformational transition in MNA · RNA consists of a widening of the nucleotide backbone with an accompanied partial unwinding of the MNA and RNA strands. This widening is most pronounced in the last three 4′-terminal base pairs, where the average distance between the P-atoms of the 2 strands increases from 17.7 Å to

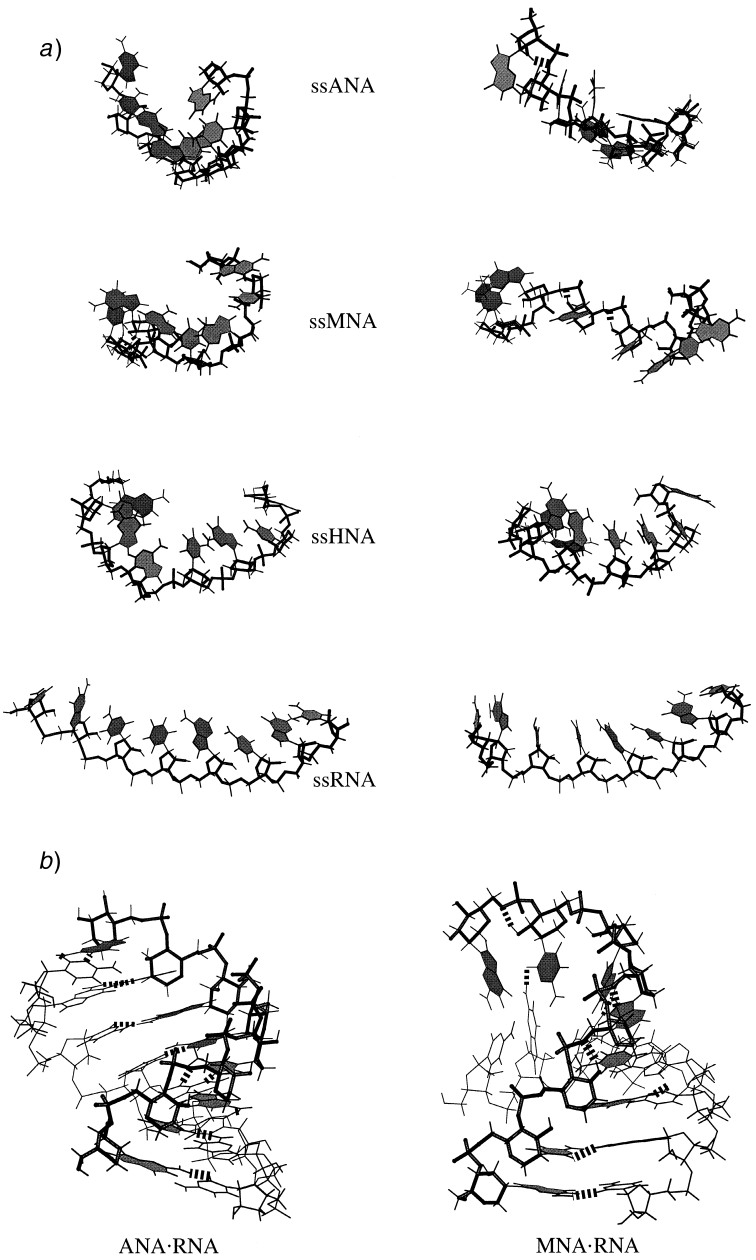

Fig. 6. a) *Snapshots of molecular structures of the single-stranded molecules at 300 ps* (left) *and 1000 ps* (right). b) *Averaged structures of the nucleic acids for the last 100 ps of simulations for the double-stranded molecules.* The phosphate-sugar backbones of ANA and MNA in the duplex structures are highlighted as sticks; H-bonds are indicated by thick dashed lines. All figures were generated with Bobscript [46][47].

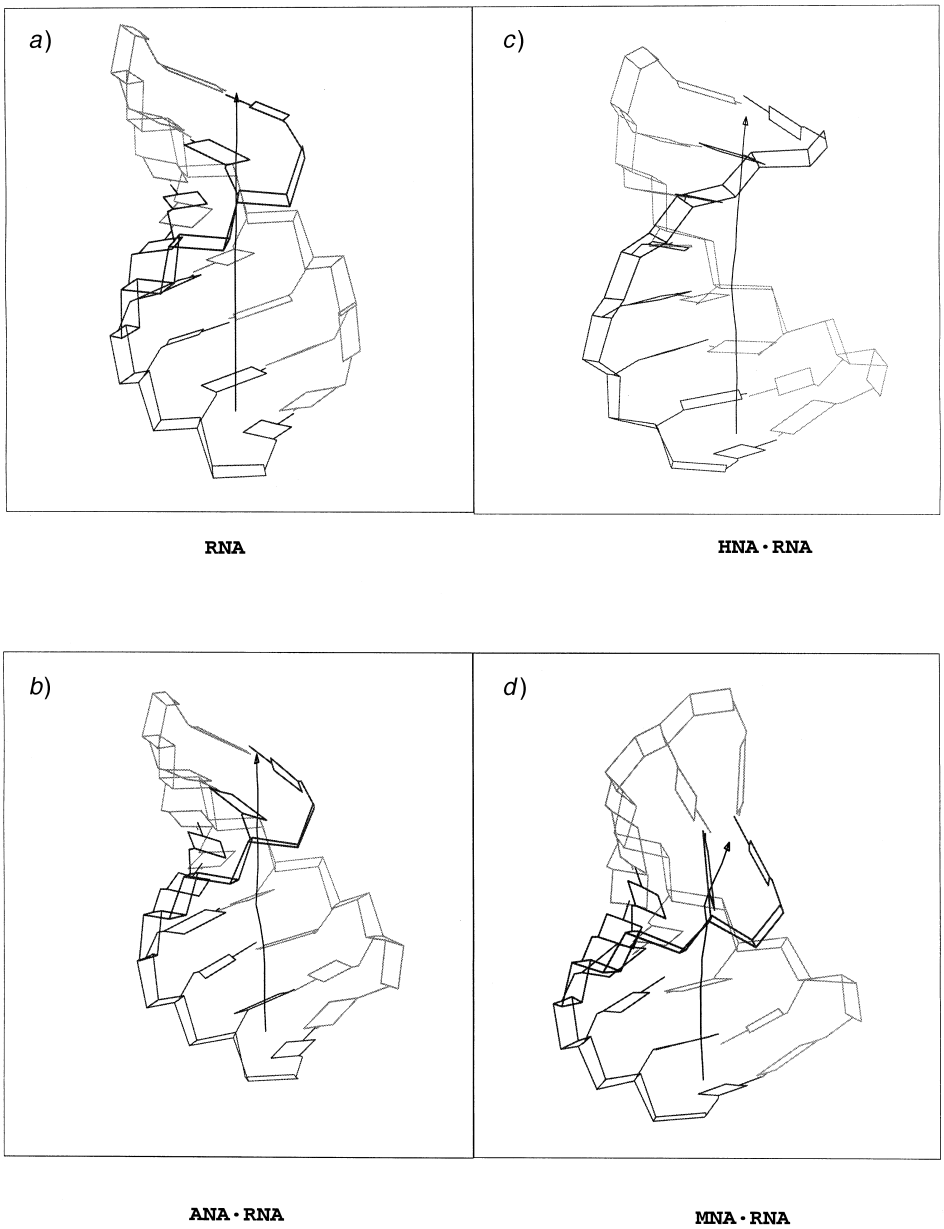

Fig. 7. *Curvature of the double helices* a) *dsRNA,* b) *ANA · RNA,* c) *HNA · RNA, and* d) *MNA · RNA as calculated by a version of the program Curves 5.0* [28], *modified to account for the six-membered sugar moieties.* The large curvature of the helical axis in the MNA · RNA system is clearly visible.

Table 2. *Average Interstrand H-Bond Lengths* (and standard deviations) *Calculated over the Last 500 ps of Each Simulation*[2]). Values in Å.

	ANA · RNA		MNA · RNA	
	Average (st. dev.)	max	average (st. dev.)	max
(G1)H1…(rC16)N3	1.99 (0.10)	2.60	2.00 (0.11)	2.93
(G1)H2B…(rC16)O2	1.94 (0.15)	2.71	1.96 (0.17)	3.36
(G1)O6…(rC16)H42	2.00 (0.18)	3.13	2.01 (0.20)	3.54
(C2)O2…(rG15)H21	1.88 (0.11)	2.57	1.89 (0.12)	2.50
(C2)N3…(rG15)H1	1.95 (0.09)	2.35	1.96 (0.11)	2.99
(C2)H4A…(rG15)O6	1.98 (0.16)	2.82	2.03 (0.21)	4.07
(G3)H1…(rC14)N3	1.96 (0.10)	2.49	1.98 (0.12)	2.89
(G3)H2B…(rC14)O2	1.87 (0.12)	2.52	1.88 (0.12)	2.81
(G3)O6…(rC14)H42	2.03 (0.19)	3.43	2.10 (0.30)	4.03
(T4)H3…(rA13)N1	1.99 (0.12)	2.66	2.04 (0.19)	3.90
(T4)O4…(rA13)H62	1.97 (0.16)	2.75	2.19 (0.31)	4.32
(A5)N1…(rU12)H3	1.97 (0.12)	2.71	2.03 (0.17)	3.40
(A5)H6A…(rU12)O4	2.13 (0.28)	3.89	2.33 (0.37)	4.10
(G6)H1…(rC11)N3	1.96 (0.09)	2.43	1.98 (0.11)	2.76
(G6)H2B…(rC11)O2	1.91 (0.13)	2.67	1.94 (0.16)	3.33
(G6)O6…(rC11)H42	1.97 (0.15)	2.84	1.99 (0.17)	3.17
(C7)O2…(rG10)H21	1.89 (0.12)	2.66	1.92 (0.14)	2.69
(C7)N3…(rG10)H1	1.95 (0.09)	2.39	1.99 (0.11)	2.68
(C7)H4A…(rG10)O6	1.96 (0.15)	2.91	2.03 (0.21)	3.36
(G8)H1…(rC9)N3	1.98 (0.11)	2.76	2.04 (0.16)	3.65
(G8)H2B…(rC9)O2	1.92 (0.15)	2.89	1.96 (0.18)	3.30
(G8)O6…(rC9)H42	2.09 (0.25)	3.77	2.09 (0.29)	4.02

18.5 Å. The conformational change also affects the minor-groove width (*Fig. 8*). In the MNA · RNA system, the minor-groove width increases from 10.5 to 11.4 Å. The HNA · RNA and ANA · RNA minor-groove widths remain fairly constant with average values of 10.2 and 10.7 Å, respectively, intermediate between the minor-groove widths of dsRNA (±11 Å) and RNA · DNA (±9 Å).

3.6. *Solvent-Accessible Surface Areas* (SASAs). Hydrophobic solvent-accessible areas can be related to the entropy of a system: when two hydrophobic molecules are put into H_2O and come together to form a dimer, the hydrophobic SASA decreases and the entropy increases by releasing structured H_2O from the hydrophobic interfaces [35]. The following empirical relation between the nonpolar SASA A and the free energy of a system was found [36]: $\Delta G = \gamma A + b$, with $\gamma = 5.0$ cal/mol Å^2 and $b =$ 0.860 kcal/mol. An increase in the hydrophobic SASA of 10 Å^2 destabilizes the system by 0.910 kcal/mol.

SASAs for the Double-Stranded Nucleic Acids. Table 3 gives the solvent accessible surface area divided into polar and hydrophobic parts. If we 'remove' the 3′-OH group of the ANA · RNA duplex and repeat the calculations, we obtain SASA contributions similar to those obtained for the HNA · RNA complex described in [6]. If we repeat this process for the MNA · RNA duplex, we do not get agreement with the HNA · RNA system.

---

[2]) A short-form notation for atoms is used to describe H-bond lengths and NMR data, *e.g.*, H1 instead of H–C (1) (see also *Fig. 1*).

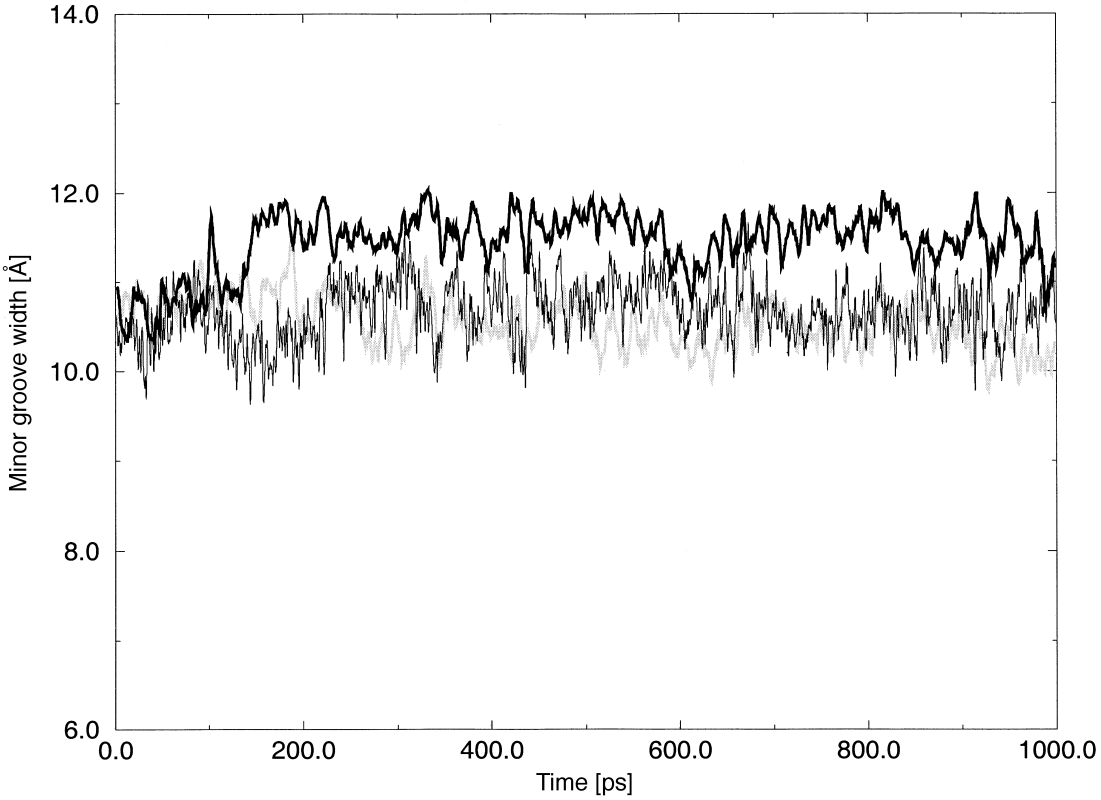

Fig. 8. *Variation of the minor-groove width as a function of time for the MNA · RNA* (black), *the ANA · RNA* (gray), *and the HNA · RNA* (thin black) *complexes.* Minor-groove widths were calculated by taking the perpendicular separations of helix strands drawn through phosphate groups diminished by 5.8 Å to account for the *van der Waals* radii of phosphate groups.

The changes in the SASA with HNA · RNA as the reference system are: polar contribution [Å^2]; +95 for ANA · RNA and +61 for MNA · RNA; hydrophobic contribution [Å^2]; −76 for ANA · RNA and +80 for MNA · RNA.

Based on these data, we conclude that ANA · RNA is better hydrated and entropically more stable (less structural H_2O over hydrophobic areas) than HNA · RNA, and that MNA · RNA is less stable than either (hydrophobic area increases more than the polar area).

SASAs for the Single-Stranded Nucleic Acids. The total hydrophobic SASA of ssMNA is larger than in ssANA, ssHNA, or ssRNA, while differences in the total polar SASAs are less pronounced (*Table 3*). The sugar and base hydrophobic SASAs for MNA are significantly larger than for ANA. These observations are a second indication for the lower stability of the MNA sugar. Except for the sugar hydrophobic component, there is remarkable similarity between the SASAs of ssANA and ssRNA.

SASAs of the 3′-OH Group. Fig. 9 shows the SASAs of the 3′-OH group during the MD simulations for both MNA · RNA and ANA · RNA. The 3′-OH group is less accessible in the MNA · RNA complex than in the ANA · RNA complex, with average

Table 3. *Decomposition of Total Solvent-Accessible Surface Area* (SASAs; in Å^2) *into Contributions of the Base, Sugar, and Phosphate Moieties, and into Contributions from Polar* (*i.e.*, O, N, and P) and Hydrophobic (*i.e.*, C) *Atoms*. Standard Deviations are given in parentheses.

	Base		Sugar		PO_4	All		
	polar	hydro-phobic	polar	hydro-phobic	polar	polar	hydro-phobic	total
ANA · RNA								
RNA	210 (11)	170 (7)	235 (6)	304 (8)	276 (5)	721 (13)	474 (12)	1195 (16)
ANA	239 (11)	158 (9)	205 (6)	393 (6)	267 (5)	711 (13)	551 (12)	1262 (20)
total	449 (21)	328 (13)	440 (9)	697 (10)	543 (7)	1432 (24)	1025 (17)	2457 (32)
MNA · RNA								
RNA	216 (8)	201 (15)	234 (9)	309 (9)	276 (5)	725 (11)	511 (21)	1236 (20)
MNA	251 (8)	209 (21)	156 (8)	462 (7)	265 (6)	673 (12)	670 (23)	1343 (28)
Total	467 (12)	410 (33)	390 (11)	771 (12)	541 (8)	1398 (17)	1181 (39)	2579 (44)
ANA · RNA [a])								
RNA	210 (11)	170 (7)	235 (6)	304 (8)	276 (4)	721 (13)	474 (12)	1195 (16)
ANA	239 (11)	160 (9)	109 (5)	468 (6)	268 (5)	615 (13)	629 (11)	1244 (20)
total	449 (21)	330 (13)	344 (8)	772 (10)	543 (7)	1336 (23)	1103 (17)	2439 (32)
MNA · RNA [a])								
RNA	216 (8)	201 (15)	234 (9)	309 (9)	276 (5)	725 (11)	511 (20)	1236 (20)
MNA	255 (8)	216 (24)	112 (5)	493 (7)	277 (6)	634 (11)	708 (26)	1342 (30)
total	470 (12)	417 (35)	346 (11)	802 (12)	543 (8)	1359 (17)	1219 (41)	2578 (45)
HNA · RNA [b])								
RNA	208 (7)	170 (8)	236 (6)	302 (8)	277 (4)	721	472	1193 (33)
HNA	237 (6)	167 (10)	113 (5)	464 (6)	266 (5)	616	631	1247 (32)
total	445 (10)	338 (14)	349 (7)	766 (10)	543 (7)	1337	1101	2440 (48)
Single strands								
ssANA	357 (10)	289 (33)	203 (7)	408 (9)	269 (5)	829 (12)	697 (37)	1526 (36)
ssMNA	362 (11)	331 (26)	193 (10)	456 (8)	267 (6)	822 (18)	787 (30)	1609 (39)
ssHNA	361 (13)	245 (18)	120 (6)	471 (9)	268 (6)	749 (17)	716 (24)	1465 (26)
ssRNA	330 (9)	282 (26)	209 (8)	332 (10)	265 (5)	804 (13)	614 (32)	1418 (31)

[a]) OH at C(3′) excluded. [b]) Values from [6].

SASAs of 46 and 106 Å^2, respectively. A polar group with low accessibility to the solvent can be unfavorable if not stabilized by other interactions. Indeed, the 3′-OH group in MNA forms intrastrand H-bonds. During the course of the simulation the SASA of 3′-OH in MNA · RNA increases slightly from about 40 to 50 Å^2, while for ANA · RNA, the SASA stays more constant.

SASAs of Minor and Major Grooves. The SASAs of the minor- and major-groove atoms were calculated for the ANA · RNA, HNA · RNA, and MNA · RNA systems (*Table 4*). All values for the HNA · RNA and ANA · RNA duplexes are very similar. With the MNA · RNA system, the minor groove becomes more accessible to the solvent, consistent with the minor-groove width calculation.

3.7. *Radial Distribution Functions around the 3′-OH Group.* Radial distribution functions g(r) of the H_2O H-atoms around O−C(3′) (*Fig. 10*) show that the H_2O around the 3′-OH group of ANA is highly structured, but that for MNA there is less structure. This is not surprising considering the SASA results, which tell us that the 3′-OH group in MNA is less accessible to the solvent than it is in ANA. The position of the first peak in the radial distribution function is at *ca.* 2.75 Å, which is typical for the

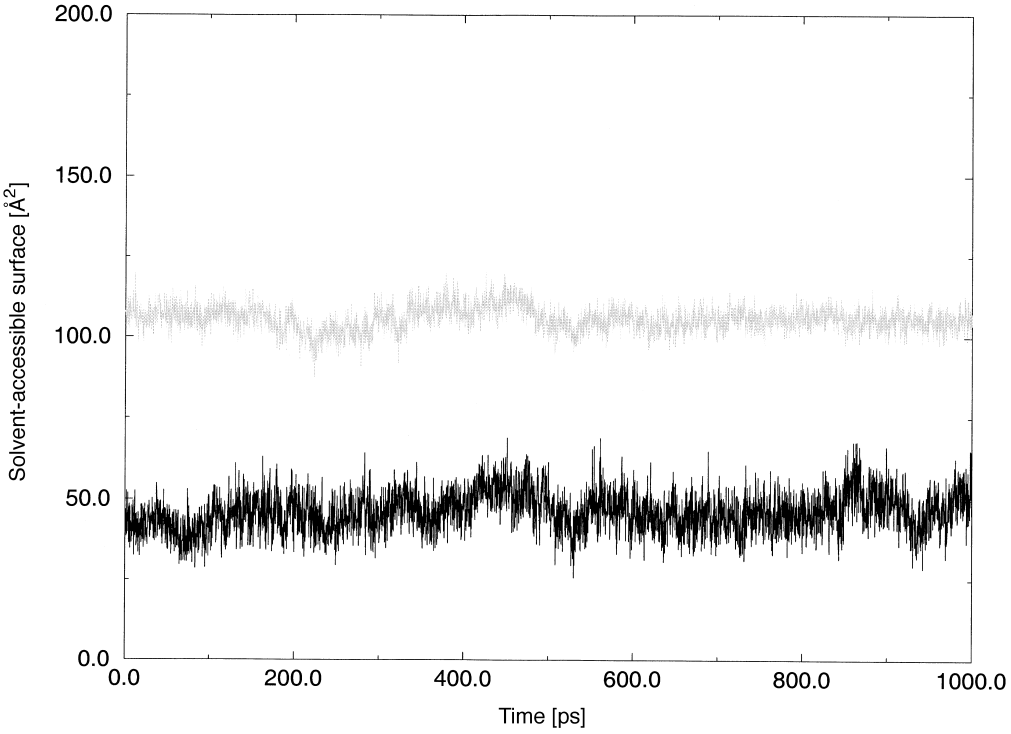

Fig. 9. *Solvent-accessible surface area* (SASA) *of the 3′-OH group as a function of the MD simulation time: ANA · RNA* (gray) *and MNA · RNA* (black)

solvation of polar species and indicates a H_2O H-bonding structure similar to that of pure H_2O [37].

3.8. *Backbone Torsion Angles and Anhydrohexitol Puckering. Single-Stranded Nucleic Acid Simulations. Table 5,a* shows the averaged torsion angles as well as the sugar-puckering parameters during the simulations. In *Fig. 11*, the evolution of the individual dihedral angles during the simulations is plotted. The differences of some selected torsion angles compared to those of the double-stranded HNA suggest that the conformational change of the MNA backbone in the double-stranded and the single-stranded simulations is similar (*Table 5,b*). From *Table 5,b*, we can also conclude that the conformational change of ssANA is different from that of ssMNA.

Table 4. *Solvent Accessible Surface Area* (SASA) *of the Minor- and Major-Groove Atoms During the Duplex Simulations, Averaged over 1000 ps.* Major-groove atoms[2]): N7, C6, and O6 of G; N4 and C5 of C; C4, O4, and C7 of T (C4, O4, and C5 of U); N7 and N6 of A. Minor-groove atoms[2]): N3 and N2 of G; C2 and O2 of C; C2 and O2 of T and U; N3 and C2 of A.

	XNA minor	XNA major	RNA minor	RNA major
ANA	118 (8)	184 (7)	118 (8)	180 (8)
HNA	117 (7)	186 (7)	117 (7)	180 (9)
MNA	138 (7)	189 (11)	135 (9)	181 (11)

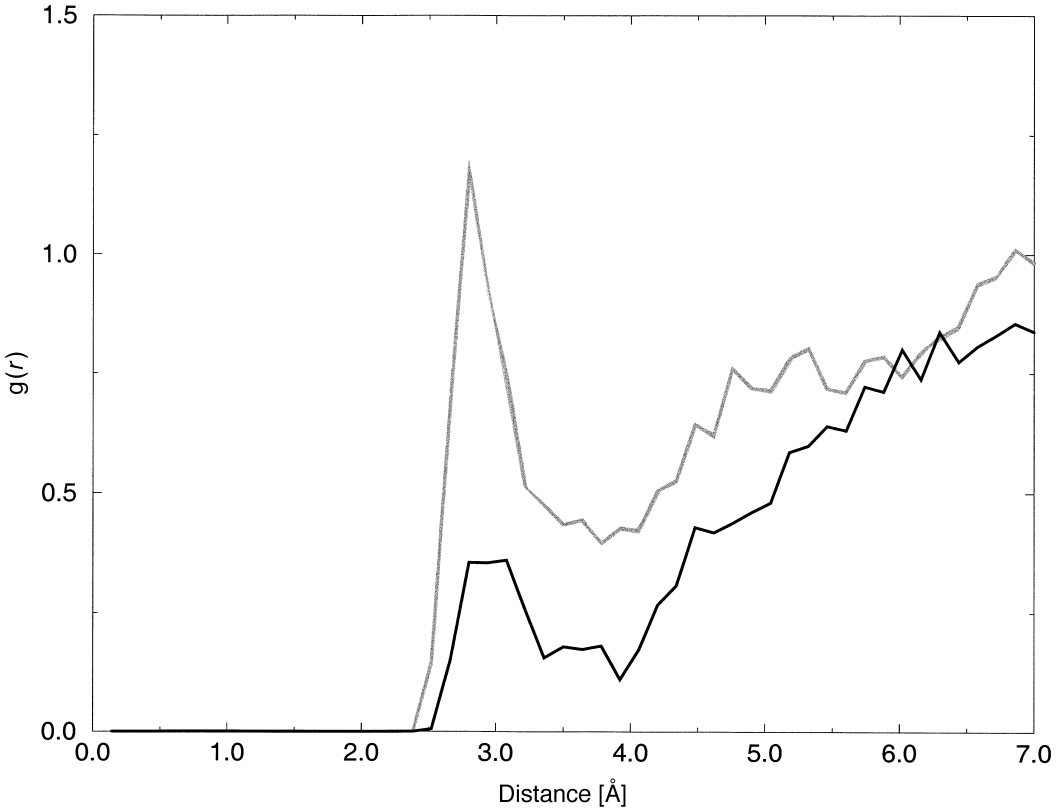

Fig. 10. *Radial distribution functions g(*r*) for H_2O H-atoms around* O–*C(3′) in ANA · RNA* (gray) *and MNA · RNA* (black). The g(*r*) were obtained by averaging over all eight 3′-OH groups with the last 100 ps of each MD trajectory. The occlusion of H_2O molecules by solute atoms was not taken into account.

The anhydrohexitol puckering phase angles in *Table 5,a* are indicative for a slightly flattened chair conformation. The high rigidity of the six-membered rings in ANA, MNA, and HNA restricts the conformational space of the single-stranded chains. The sugars of the free RNA chain remain close to the C(3′)-*endo* conformation ($P \approx 18°$), even after unfolding of the oligomer.

Double-Stranded Nucleic Acid Simulations. Table 6 shows the torsion angles and sugar-puckering parameters. The ANA · RNA and HNA · RNA duplexes show values that are comparable with those of the canonical A-family of oligonucleotide structures [38]. The instability of the MNA · RNA system is confirmed by the higher standard deviations for the torsion angles α, ε, and χ in the MNA strand and for ε and χ in the RNA strand.

3.9. *Intrachain Hydrogen-Bonding Patterns: Single Strands. Fig. 12* shows the intrastrand H-bonds from the 3′-OH group in the ANA and MNA single-strand simulations. The single-stranded MNA is stabilized by frequent H-bonds between OH–C(3′) and O–C(6′) in the phosphate backbone of the following nucleotide. With the single-stranded ANA simulation, the H-bond OH–C(3′) to O–C(4′) at the same nucleotide is more frequent, although the pattern is not quite so striking.

Table 5. a) *Torsion Angles of the Single-Stranded Chains, with Standard Deviations in Parentheses, Averaged over 1000 ps and over All the Residues* (the first value in each entry results from the calculation excluding the two terminal residues (a/m/hG1 and a/m/hG8 of a-, m-, or h(GCGTAGCG) and rC9 and rC16 of r(CGCUACGC), the second value from the calculation including all residues) *and* b) *Differences of Some Selected Torsion Angles Compared to Those of Double-Stranded HNA*. Torsion Angles are defined in *Fig. 3*.

a)	ANA	MNA	HNA	RNA
α	268 (44)	246 (65)	253 (69)	275 (10)
	278 (10)	271 (13)	281 (12)	274 (10)
β	173 (11)	176 (28)	173 (17)	177 (10)
	171 (10)	171 (31)	168 (10)	177 (9)
γ	76 (35)	108 (58)	77 (39)	70 (28)
	75 (29)	101 (54)	83 (43)	66 (9)
δ	78 (30)	80 (30)	80 (27)	91 (20)
	67 (7)	69 (7)	70 (7)	84 (8)
ε	210 (18)	226 (15)	222 (22)	190 (12)
	207 (17)	226 (14)	216 (17)	189 (10)
ζ	282 (15)	280 (11)	280 (30)	276 (10)
	283 (12)	281 (9)	286 (11)	276 (9)
χ	227 (16)	231 (17)	224 (17)	228 (59)
	224 (11)	233 (15)	224 (11)	243 (17)
Q, q [Å]	0.525 (0.039)	0.532 (0.039)	0.523 (0.040)	0.333 (0.063)
	0.521 (0.038)	0.532 (0.039)	0.522 (0.040)	0.330 (0.058)
θ [°]	29.4 (52.2)	30.1 (52.4)	29.9 (51.4)	
	9.8 (5.0)	10.4 (5.5)	10.4 (5.4)	
φ [°]	171.0 (118.6)	157.6 (111.9)	163.3 (106.2)	
	164.2 (116.3)	145.4 (111.9)	151.4 (105.0)	
P [°]				32.1 (52.8)
				15.4 (17.4)

b)	Torsion	dsHNA	dsANA	dsMNA	ssHNA	ssANA	ssMNA
	$\Delta\alpha$ [°]	0	−2	−13	−1	−4	−11
	$\Delta\varepsilon$ [°]	0	−1	+10	+4	−5	+14
	$\Delta\zeta$ [°]	0	0	−7	−2	−5	−7

Double Strands. Fig. 13 shows the major intrastrand H-bonds in the ANA and MNA strands during the duplex simulations. In MNA·RNA, OH−C(3′) forms mainly H-bonds with O−C(5′) and O−C(6′) from the next nucleotide in the chain. In ANA·RNA, a strong H-bond is made from OH−C(3′) to O−C(4′) of the same nucleotide and less frequent H-bonds are made to O−C(5′) and O−C(6′) of the next nucleotide. This pattern is similar to that seen with single-stranded ANA, but more pronounced.

3.10. *Adiabatic Torsional-Energy Maps: α,ζ Energy Maps.* The major flexibility in a polynucleotide backbone resides primarily in the internucleotide P-O links [39]. This flexibility can be monitored by the angles α and ζ (*Fig. 3*). Therefore, energy maps as a function of those two angles were calculated for the dinucleotides G_hpC_h, G_apC_a, and G_mpC_m as models for HNA, ANA, and MNA, respectively (*Fig. 14*). It is observed that the valleys in G_apC_a and G_mpC_m are steeper and deeper than in the G_hpC_h case. To go to the valley in the lower-right region of the map, G_apC_a has to cross a barrier of *ca.* 10 kcal/mol, while G_hpC_h has to surmount only 5 kcal/mol. Further analysis of these dinucleotides shows that G_apC_a and G_mpC_m have intrastrand H-bonds between O−C(3′) and other atoms like O−C(5′), O−C(6′), O−C(4′), OP(1), and OP(2) (data not shown) that restrict the G_mpC_m and G_apC_a chains in their movement and may

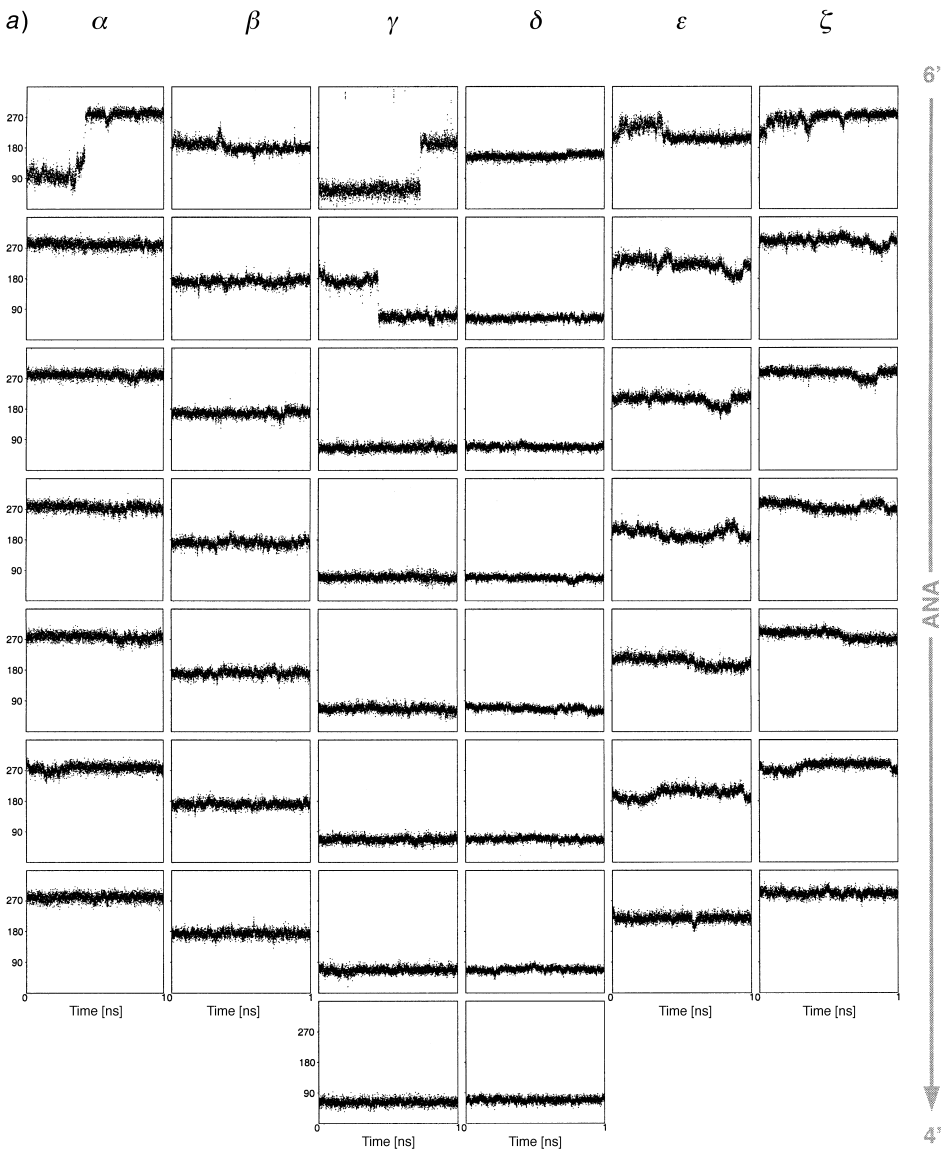

Fig. 11. *Evolution of all the torsion angles in the single-stranded simulations:* a) *ssANA*, b) *ssMNA, and* c) *ssHNA*

explain steeper valleys in the energy map. From these observations, it can be concluded that the higher rigidity of the backbone of ANA (due to a more conformational restriction of torsion angle ζ) may contribute to the favorable entropy of duplex formation and thus to more stable hybrids.

ε,ζ Energy Maps. To investigate the possible interaction of the 3′-OH groups with the backbone in ANA and MNA, adiabatic energy maps of the dinucleotides G_hpC_h, G_apC_a, and G_mpC_m were calculated as a function of the torsion angles ε and ζ. The

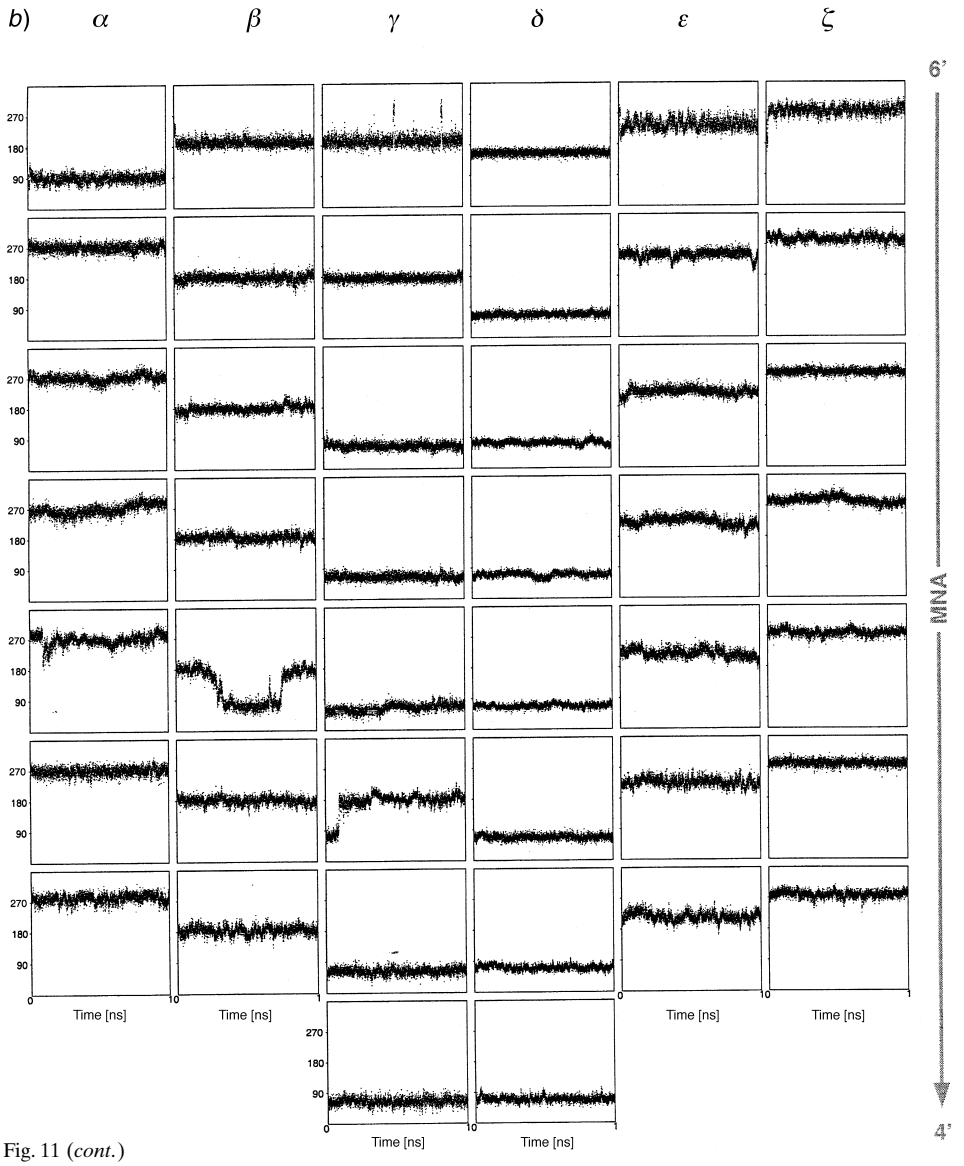

Fig. 11 (*cont.*)

resulting maps (data not shown) did not show contributions from steric interaction between the 3′-OH groups and the backbone in either G_mpC_m or G_apC_a.

3.11. *Structural Studies of an ANA · RNA Complex by NMR Spectroscopy.* The modeling calculations furnished similar structures for the ANA · RNA and HNA · RNA duplexes. To verify these results in an experimental way, an NMR study was performed on the ANA · RNA complex [6′-a(GCGUAGCG)-4′] · [3′-r(CGCAUCGC)-5′] and the data obtained were compared to those measured for the HNA · RNA complex [6′-h(GCGTAGCG)-4′] · [3′-r(CGCAUCGC)-5′] [40].

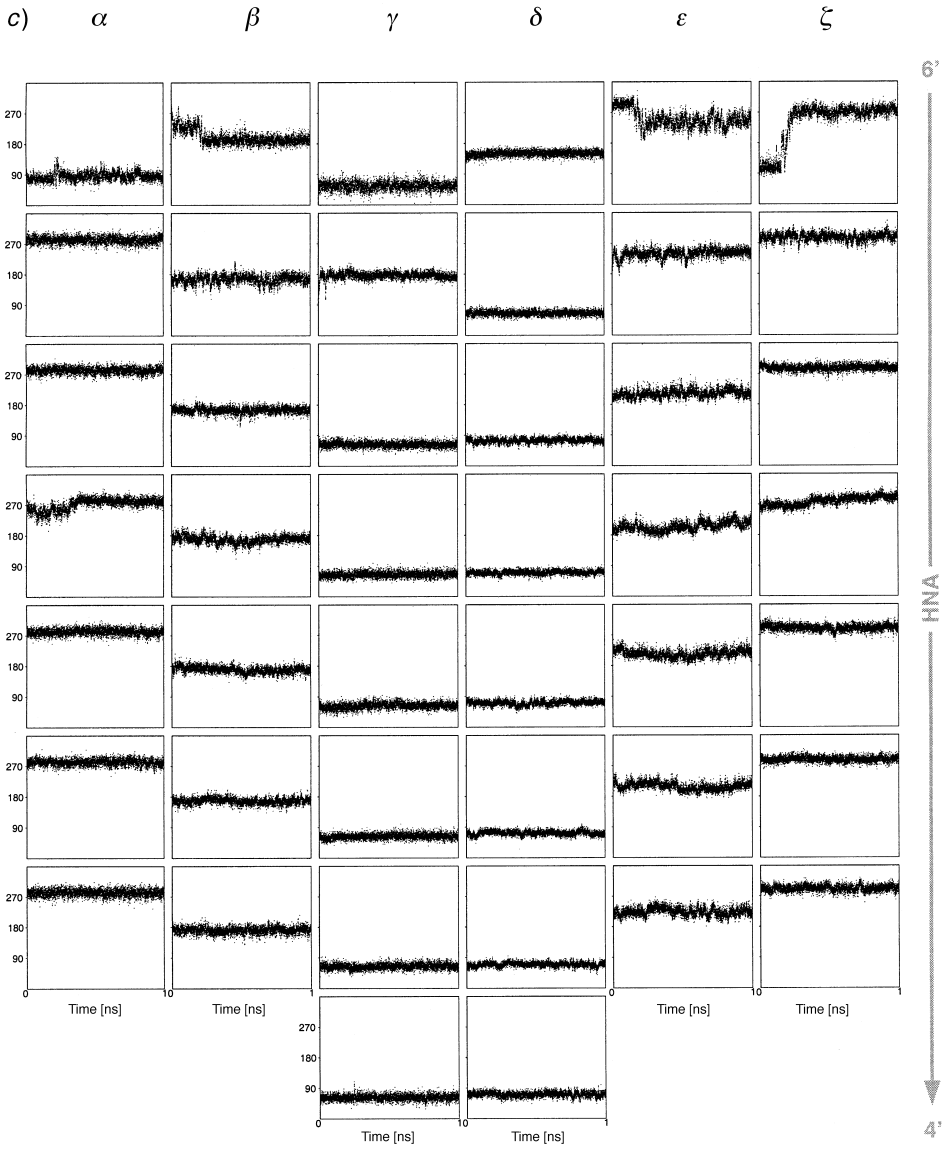

A 1D ^{1}H-NMR spectrum of a(GCGUAGCG) revealed the complexity of an NMR study for the ANA · RNA duplex. At 20°, the ^{1}H-NMR spectrum of a(GCGUAGCG) (1 mM in H_2O/D_2O 9:1) shows strong imino signals in the region 12–14 ppm and extreme broadening of all signals, indicating strong intermolecular interaction of ANA strands under the experimental conditions used. At 50°, line broadening is no longer observed, but strong signal overlap is visible in the region around the H_2O signal between 4.00 and 5.00 ppm, where all 64 signals of the altritol-ring protons occur. The high degree of overlap in this region of the ^{1}H-NMR spectrum, combined with the high

Table 6. *Torsion Angles and Puckering Parameters of the Duplexes, with Standard Deviations in Parentheses, Averaged over 1000 ps and over All the Residues* (the first value in each entry results from the calculation excluding the four terminal residues a/m/hG1 and a/m/hG8 of a-, m-, or h(GCGTAGCG) and rC9 and rC16 of r(CGCUACGC), the second value from the calculation including all residues). Torsion angles are defined in *Fig. 3*.

	ANA · RNA		MNA · RNA		HNA · RNA [a])	
	ANA strand	RNA strand	MNA strand	RNA strand	HNA strand	RNA strand
α	253 (68)	280 (11)	244 (70)	278 (11)	267 (54)	280 (11)
	280 (9)	280 (10)	269 (19)	278 (11)	282 (9)	280 (10)
β	178 (26)	176 (10)	184 (24)	178 (12)	183 (55)	176 (11)
	169 (9)	174 (10)	176 (10)	176 (11)	175 (10)	175 (10)
γ	86 (48)	79 (38)	81 (38)	69 (24)	83 (44)	66 (10)
	86 (44)	66 (9)	87 (42)	65 (11)	81 (39)	66 (10)
δ	80 (29)	84 (18)	82 (25)	86 (19)	81 (28)	84 (19)
	69 (6)	79 (6)	72 (7)	80 (7)	71 (7)	78 (7)
ε	216 (16)	203 (11)	228 (25)	203 (13)	220 (24)	203 (11)
	211 (10)	203 (11)	222 (12)	204 (14)	212 (11)	203 (11)
ζ	276 (34)	290 (9)	260 (53)	288 (10)	276 (42)	289 (9)
	288 (7)	291 (8)	281 (8)	288 (10)	–	–
χ	230 (19)	207 (12)	243 (28)	215 (18)	243 (22)	211 (14)
	224 (8)	204 (10)	231 (16)	213 (19)	235 (14)	209 (13)
Q, q [Å]	0.519 (0.038)	0.380 (0.058)	0.523 (0.041)	0.371 (0.060)	0.520 (0.041)	0.381 (0.058)
	0.516 (0.038)	0.386 (0.053)	0.522 (0.041)	0.375 (0.059)	0.517 (0.041)	0.387 (0.054)
θ [°]	29.2 (52.9)		30.1 (49.3)		29.5 (51.3)	
	9.3 (4.8)		11.0 (5.9)		10.3 (5.4)	
φ [°]	152.1 (104.7)		140.7 (97.2)		155.0 (105.6)	
	141.2 (99.3)		125.2 (88.4)		142.0 (102.5)	
P [°]		30.6 (42.4)		34.6 (44.7)		31.1 (43.0)
		17.1 (11.1)		19.1 (14.0)		17.3 (11.5)

[a]) Values from [6].

degree of overlap in the ^{31}P-NMR spectrum, hampered a full assignment and structure calculation of the ANA · RNA duplex without isotopic enrichment.

A sample of an a(GCGUAGCG) · r(CGCUACGC) duplex was prepared by adding small amounts of ANA to an RNA solution in D_2O (1.05 mM). The titration was followed by 1D ^{1}H-NMR spectroscopy after each addition of ANA. A small amount (5%) of RNA was used in excess to prevent self-association of the ANA strands. However, while all RNA signals had normal linewidths (*ca.* 1 Hz) at 20°, all ANA signals were broadened. Increasing the temperature to 50° prevented the line broadening of the ANA signals. At this high temperature, the anomeric-to-aromatic proton walk in the RNA strand is visible (*Fig. 15*, *a*) in a NOESY plot with mixing time 150 ms, but the cytosine H5 to H6^2) cross-peaks in the single-stranded RNA are increased, and exchange cross-peaks between the single-stranded RNA and RNA in the duplex occur (marked with shaded box and X, respectively). Except for the slight shift of the (rC1)H6 and (rC8)H6 signals, the spectra of the ANA · RNA sample at 20 and 50° are very similar (*Fig. 15*, *a* and *b*). In both experiments, the RNA strand shows sharp H1′ signals, strong intraresidue H8(n) or H6(n) to H3′(n) and strong interresidue H8(n) or H6(n) to H2′(n – 1) NOE cross-peaks. These are typical characteristics for

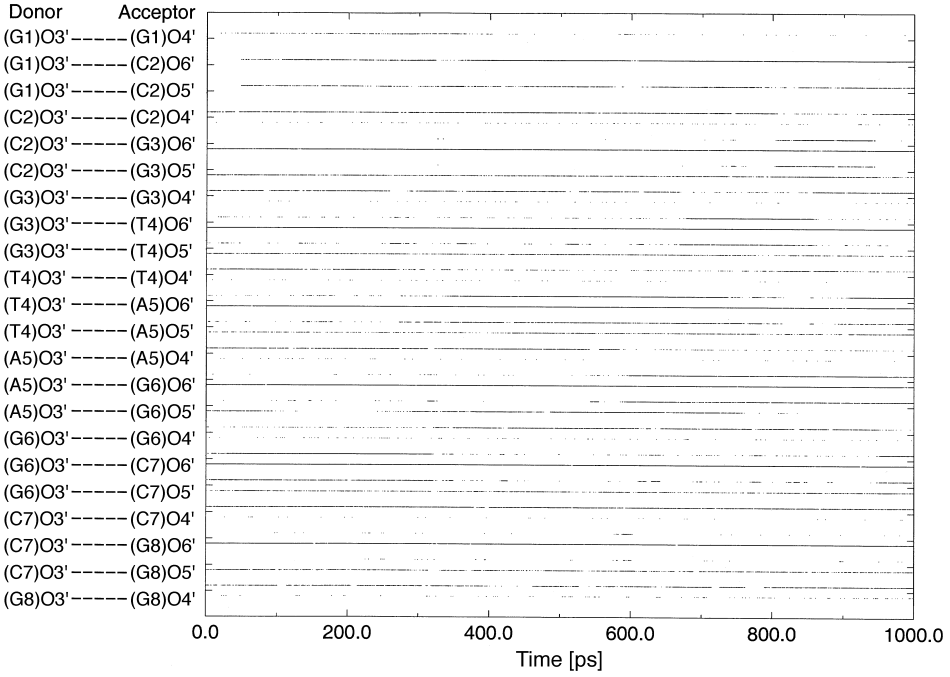

Fig. 12. *Hydrogen bonds of OH–C(3′) in single-strand ANA and MNA during the MD simulations*[2]). The presence of 22 possible H-bonds during the course of the simulations is indicated by dots. There are two curves for every H-bond, the upper curve is for ANA, while MNA is represented by the lower curve. Plots were generated with xmgr software [48].

RNA in A-type dsRNA structures with *N*-type ribose sugars [41]. The interstrand NOE cross-peak from (rA13)H1′ to (aA5)H2 (marked with *) is an indication for a minor groove comparable to the one in A-type helices [42]. The ^{31}P-NMR chemical shifts (-3.05 to -3.85 ppm) are also typical for A-type helices [43].

Because of the spectral overlap of the altritol ^{1}H-NMR signals, it was not possible to do a sequential assignment in the ANA strand, neither by a NOE pathway, nor by a ^{1}H-detected ^{1}H,^{31}P-HETCOR experiment. The resonances of aromatic- and anomeric-proton signals of the ANA · RNA sample were compared to the assigned signals of an HNA · RNA duplex measured at 20° [40]. The anomeric to aromatic proton walk of the RNA strand in this latter duplex is similar to the one of the ANA · RNA sample (*Fig. 15*, *c*), indicating that there are no fundamental structural differences in the RNA part of both duplexes. The aromatic-proton signals that do not belong to RNA in the ANA · RNA sample have chemical shifts close to the H8, H6, H5, and H2 signals of the HNA strand in the HNA · RNA duplex (*Table 7*). Since there is only a small difference in the RNA part of both duplexes, this resemblance in chemical shift was used to sequentially assign the aromatic signals of the A_a, G_a, and C_a residues. The remaining unassigned signals belong to H6 and H5 of the uracil residue present in the ANA strand where the HNA strand contains a thymine residue.

At 50° and mixing time 150 ms, it is possible to distinguish two strong NOEs from the resolved aromatic ANA signal to protons in the region 4.10–4.70 ppm, except for

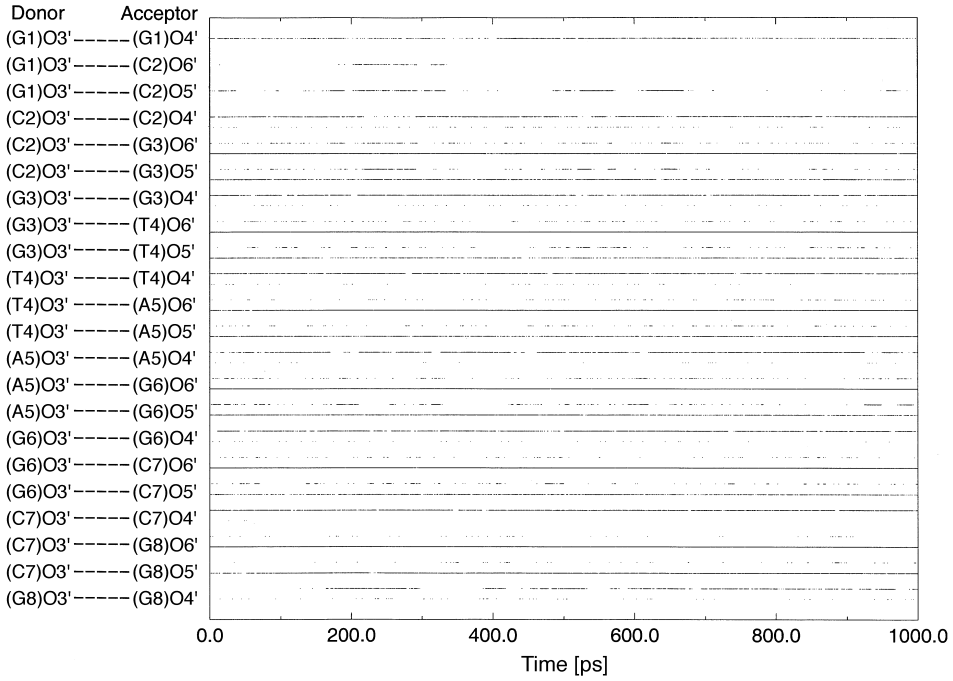

Fig. 13. *Hydrogen bonds of OH–C(3′) in the MNA and ANA strand during the MNA · RNA and ANA · RNA MD simulations.* The presence of 22 possible H-bonds during the course of the simulations is indicated by dots. There are two curves for every H-bond, the upper curve is for ANA, while MNA is represented by the lower curve.

the signal at 8.19 ppm with only one cross-peak. We were not able to assign cross-peaks for (aC2)H6 and (aU4)H6 that are overlapping with (rG10)H8 at 7.9 ppm. Assuming that altritol rings in ANA and hexitol rings in HNA adopt similar conformations when duplexed with their RNA complements, one of these cross-peaks can be assigned to an intraresidue interaction from H8 or H6 of the nucleobase to H4′ of the altritol ring. The second cross-peak is a sequential NOE from H8 or H6 of the nucleobase in one residue (n) to H4′ of the altritol ring in the previous residue ($n-1$). For the first residue in the ANA strand ((aG9)H8 at 8.19 ppm), this second cross-peak is absent. A ^{1}H-detected ^{1}H,^{31}P-correlation experiment was performed to confirm the assignment of the H4′ protons in ANA. However, due to extreme signal overlap in the ^{1}H-dimension (4.70–4.10 ppm) as well as ^{31}P-dimension (-3.05 to -3.85 ppm), it was impossible to resolve the cross-peaks. Comparison of the assignments for the H3′ and H4′ resonances in ANA to those in HNA (*Table 7*) demonstrates again the similarity in chemical shifts of the H4′ signals, while the H3′ signals are shifted downfield due to the deshielding effect induced by the 3′-OH group in ANA. In conclusion, the NMR data sustain the modeling observation that the structure of the HNA · RNA and ANA · RNA duplexes are very similar.

4. Discussion. – The replacement of the D-furanose moiety of a nucleoside with an anhydro-D-hexitol ring has led to the discovery of a new series of nucleic acids with

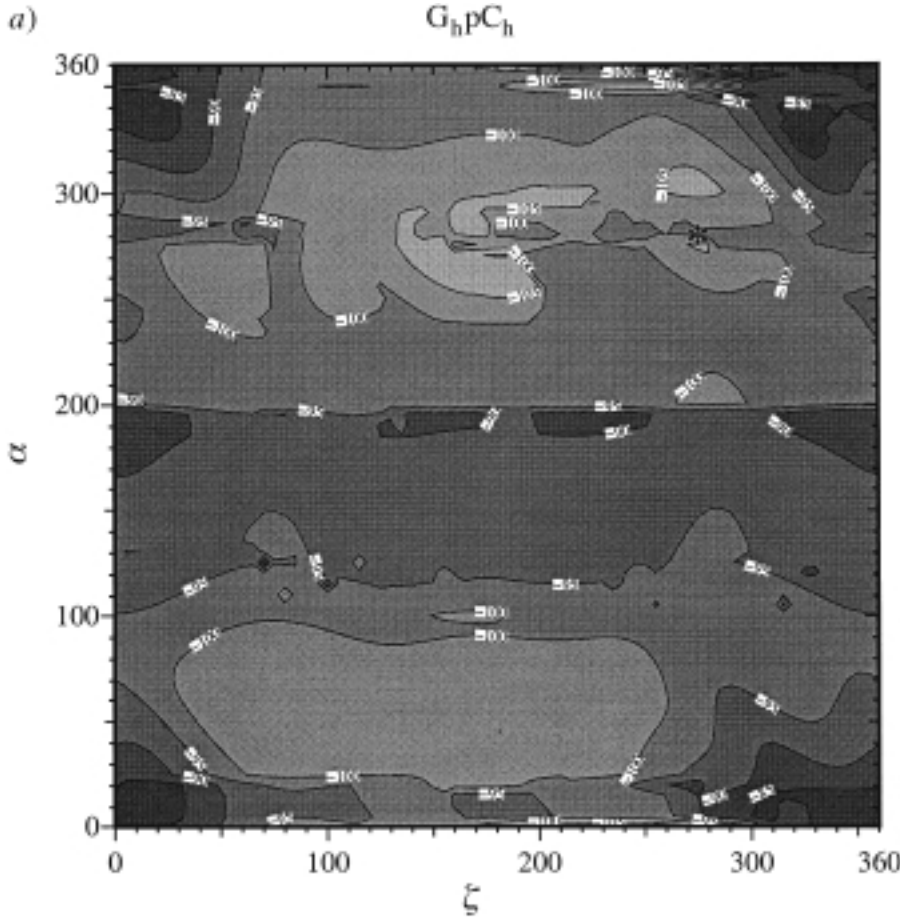

Fig. 14. *Two-dimensional adiabatic energy contour maps as a function of the torsion angles α and ζ for model dinucleotides of HNA, ANA, and MNA*: a) G_hpC_h, b) G_apC_a, *and* c) G_mpC_m, *respectively.* The torsion angles γ, β, and ε were kept constant at 81, 167, and 212°, resp., during the calculations. The asterisks in the figures mark the average duplex conformations during the MD simulations. The figures were created with Plotmtv [49].

specific hybridizing properties. The prototype HNA (=D-hexitol nucleic acid without 3′-OH group) is a *Watson-Crick*-type self-pairing system and, in addition, hybridizes strongly with natural RNA. The higher stability of dsHNA and HNA · RNA duplexes (when compared with dsRNA and DNA · RNA) is attributed to the higher preorganization of single-stranded HNA, enhanced by efficient stacking interactions. Due to this preorganization, HNA is an efficient template for nonenzymatic synthesis of RNA. The potential of HNAs as antisense oligonucleotides has recently been described [44].

When considering the minor-groove structure of a HNA · RNA duplex, we observed a large difference in the polarity of the solvent-accessible surface between the RNA and HNA flanks. While the RNA flank is well hydrated due to the presence of the 2′-OH group, the HNA flank is very hydrophobic and less well-hydrated (due to the absence of the 3′-OH group). This might result in a low entropy of H_2O molecules in

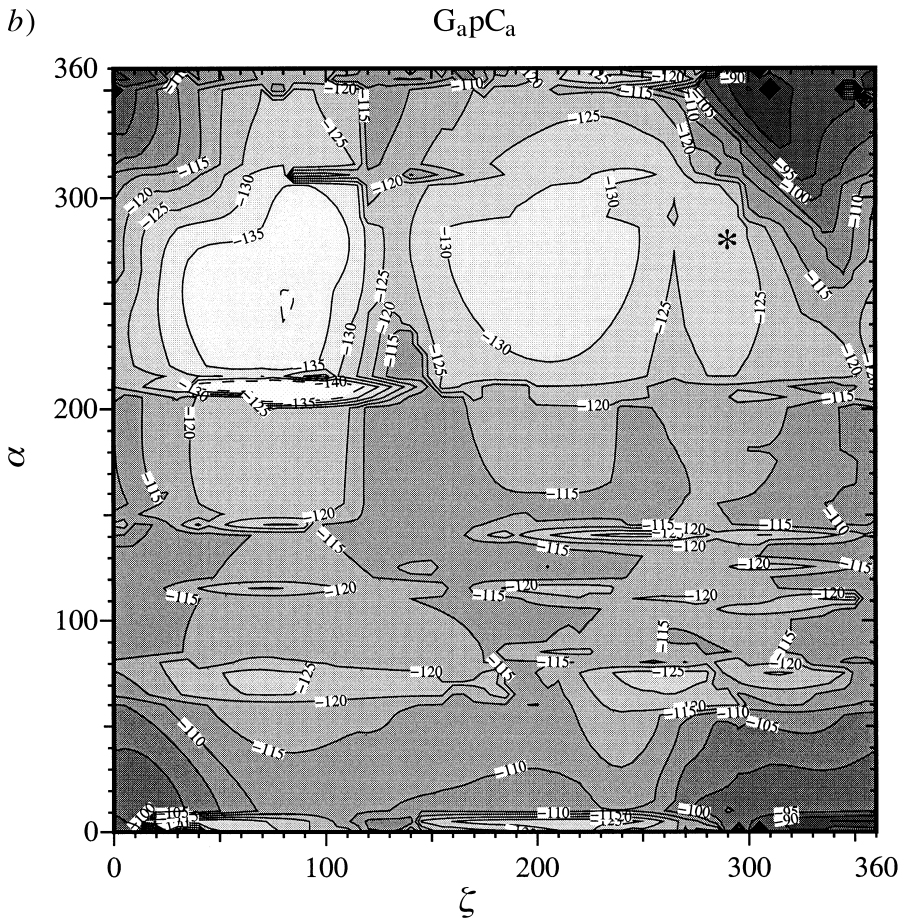

Fig. 14 (*cont.*)

the neighborhood of the HNA flank, which is an unfavorable thermodynamic situation. Therefore, we reasoned that an increase in the polarity of the solvent-accessible surface might be beneficial for hydration and hybridization. This can be achieved by the introduction of an OH group at the 3′-position of HNA.

When an OH group is introduced at the 3′β position, D-mannitol nucleic acids (MNAs) are obtained. This modification is detrimental for hybridization properties. Introduction of an OH group in the 3′α position gives D-altritol nucleic acids (ANAs). ANA hybridizes more strongly with RNA than does HNA. Experimentally, the following order of complex stability is observed ANA · RNA > HNA · RNA > RNA · RNA > MNA · RNA [15]. At first sight, the difference between the stability of ANA · RNA and HNA · RNA can be attributed to better hydration of the former duplex. In this work, we have tried to explain this difference by MD simulation techniques and analysis of several parameters that can play a role in duplex stabilization.

Preorganization of an oligomer may favor duplex stability due to a low entropy penalty upon hybridization. A prerequisite for this is that the conformation of the

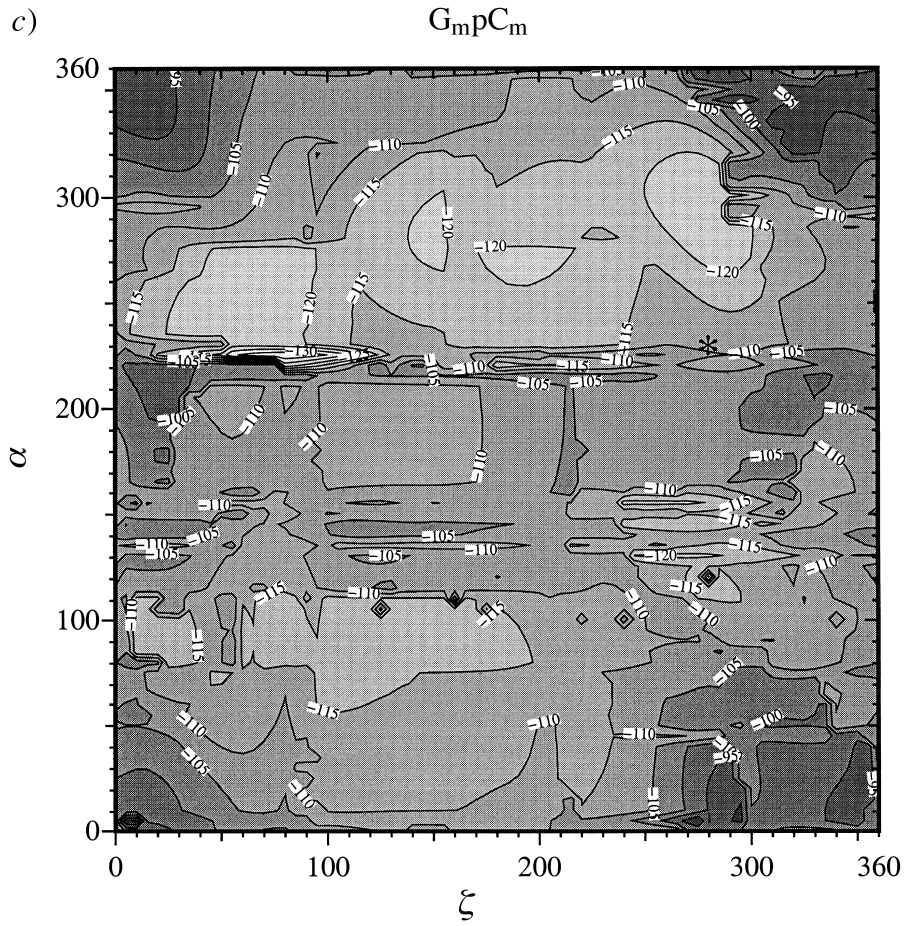

Fig. 14 (*cont.*)

preorganized single-stranded oligonucleotide is similar to its conformation in the duplex. From *Fig. 5*,*b* we concluded that the HNA, ANA, and MNA strands are conformationally more preorganized than RNA in the single-strand simulations. The six-membered hexitol ring is less flexible than the five-membered ribose ring. Puckering transitions in five-membered rings occur easily and are almost continuous (if not restricted by interactions of substituents), which explains the higher flexibility of the RNA chain [38]. Six-membered rings occur almost exclusively in one of the two chair forms, and transition to the other form is not always easy, especially when large substituents are present. This is the case for the six-membered rings of HNA, ANA, and MNA. In all three cases, the most stable conformation of the six-membered hexitol ring is a chair conformation with an axially oriented base moiety. In this conformation, the hexitol nucleosides can be considered good mimics of a furanose nucleoside in its C(3′)-*endo* conformation, and this is the conformation of the furanose sugar found in an A-RNA-like helix. The stability of the axial base conformation in the oligomer is

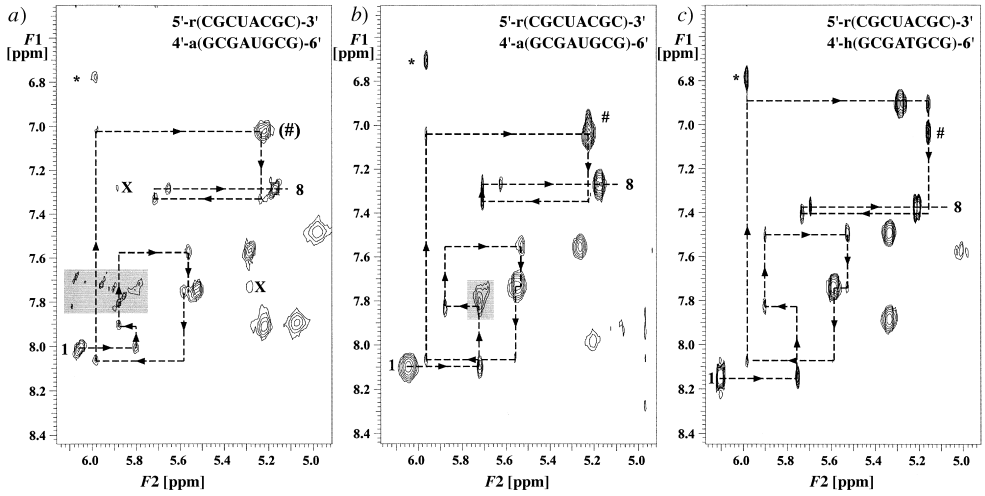

Fig. 15. *Expansion of a NOESY plot measured with mixing time 150 ms* a) *at 50° for ANA · RNA,* b) *at 20° for ANA · RNA, and* c) *at 20° for HNA · RNA showing the anomeric-to-aromatic proton walk in the RNA part of the complexes* (start and end are marked with 1 and 8, resp.). Cross-peaks from the excess RNA are enclosed in a shaded box. Assignment of the marked cross-peaks[2]): exchange crosspeak (X), interstrand (aA5)H2 or (hA5)H2 to (rA13)H1′ (*), intrastrand (rA13)H2 to (rC14)H1′ (#).

confirmed by the single-stranded HNA, ANA, and MNA simulations where, throughout the 1000 ps simulation, the hexitol ring remains in the $^4C_1$ conformation with the base moiety axially oriented. The $^4C_1$ conformation as well as the helical form of the single-stranded HNA, ANA, and MNA are further stabilized by additional interactions like base-base stackings. This preorganization in an A-type helix is due to the fact that the δ torsion angle is frozen at 80 degrees [45], the mean value found in A-DNA. This δ torsion angle is determined by the conformation of the hexitol ring. The double-stranded simulations confirm this hypothesis.

The less flexible HNA and ANA single strands get easily preorganized in an A-type helix conformation, and the more flexible RNA strand fits easily to this preformed molecule. In the single-strand simulations, it is observed that ANA unfolds slowly by a decrease of the dihedral angles α, ε, and ζ. We expect the single-stranded HNA to behave similarly or at least a major change of one dihedral angle, like the very flexible α or ζ, could be expected. However, this behavior is not observed, even when continuing the simulation up to 2000 ps (data not shown). We postulate that the single-stranded ANA and HNA chain exist in a semi-random conformation, which can easily be converted to an A-like helical conformation by small changes of some dihedral angles of the main chain. We do not observe a perfect preorganization in the way as defined above. However, the rigid sugar conformation may limit the conformational freedom of the ssHNA and ssANA to a narrow conformational space. For both structures, the A-conformation is statistically more accessible than in the case of ssRNA where the conformational space is much more expanded.

The MNA single strand is likewise preorganized but in a more aberrant conformation (see below). This conformation is less complementary for RNA and requires too drastic a change to keep the double-stranded MNA · RNA helix together

Table 7. *Assigned ^{1}H-NMR Chemical Shifts* [ppm] *of the ANA · RNA Duplex at 20 and 50°* (first and second line for each residue, resp.) *Compared to the Assigned Corresponding Chemical Shifts of HNA · RNA Duplex at 20°* (third line)[2]). Acetate was used as internal reference (= 1.92 ppm).

	T [°]	H8 or H6	H2 or H5	H3′1	H3′2	H4′		T [°]	H8 or H6	H2 or H5	H1′	H2′	H3′
aG1	20	8.22	–	–			rC9	20	8.10	6.04	5.72	4.64	4.61
	50	8.19	–	–		4.24		50	8.01	6.06	5.80	4.62	4.61
hG1	20	8.21	–	2.24	2.77	4.28		20	8.14	6.10	5.74	4.65	4.63
aC2	20	7.99	5.20	–			rG10	20	7.84	–	5.88	4.59	4.65
	50	7.91	5.22	–	4.65			50	7.91	–	5.88	4.62	
hC2	20	7.88	5.33	2.08	2.90	4.59		20	7.82	–	5.90	4.61	4.65
aG3	20	7.96	–	–			rC11	20	7.55	5.26	5.53	4.36	4.48
	50	7.95	–	–		4.44		50	7.57	5.29	5.57	4.35	4.47
hG3	20	7.88	–	2.12	2.85	4.32		20	7.48	5.33	5.52	4.38	4.45
aU4	20	7.92	5.07	–			rU12	20	7.74	5.54	5.56	4.43	4.58
	50	7.90	5.07	–	4.62			50	7.75	5.52	5.58	4.41	4.58
hT4	20	7.79	1.27	2.08	2.95	4.65		20	7.73	5.58	5.59	4.45	4.58
aA5	20	8.40	6.72	–			rA13	20	8.06	6.98	5.96	4.45	4.61
	50	8.38	6.78	–	4.61	4.58		50	8.06	7.02	5.98	4.42	4.60
hA5	20	8.36	6.78	2.16	2.86	4.55		20	8.07	7.03	5.98	4.54	4.61
aG6	20	7.29	–	–			rC14	20	7.05	5.22	5.23	4.37	4.23
	50	7.25	–	–	4.40	4.24		50	7.02	5.22	5.24	4.35	4.22
hG6	20	7.35	–	1.95	2.68	4.26		20	6.90	5.28	5.16	4.35	4.15
aC7	20	7.57	4.91	–			rG15	20	7.35	–	5.71	4.49	4.35
	50	7.48	4.89	–	4.47	4.32		50	7.34	–	5.71	4.48	4.35
hC7	20	7.57	5.01	1.91	2.85	4.36		20	7.41	–	5.73	4.54	4.61
aG8	20	7.75	–	–			rC16	20	7.27	5.18	5.62	4.00	4.05
	50	7.78	–	–		4.14		50	7.29	5.17	5.65	4.02	4.05
hG8	20	7.79	–	2.05	2.31	4.28		20	7.37	5.21	5.69	4.01	4.11

in a stable way. The high preorganization and the restricted movement of ANA and MNA may explain why they are excellent, chirally selective templates for non-enzymatic oligonucleotide synthesis [10–12].

From the point of view of conformational preorganization, the flexibility of ANA and MNA is even more restricted than that of HNA, as can be seen from the adiabatic energy maps of the model dinucleotides (*Fig. 14*). Due to interactions of the 3′-OH group with O–C(6′) in the backbone and frequent H-bonds with O–C(5′) (*Fig. 12* and *13*), the conformational space is more limited for MNA and ANA in comparison to HNA (which lacks the 3′-OH group). The higher standard deviations in the ζ dihedral angle in ssHNA compared to ssANA and ssMNA may also be a sign of the higher flexibility of HNA.

As mentioned above, MNA seems to preorganize in a conformation that is significantly different from the normal helical A or B type. Frequent H-bonds occur between the 3′-OH group and O–C(6′) in the phosphate backbone of the following nucleotide, as well as the double-stranded and the single-stranded simulations. This H-bond pattern does not stabilize a normal A- or B-type helical structure. On the contrary, for the double-stranded MNA · RNA complex, a conformational change occurs whereby the nucleotide backbone widens and the MNA · RNA strand partially

unwinds (*Fig. 6,b*). This widening is most pronounced in the last three (4′-terminal) base pairs. Several observations support such a structural alteration.

The deformation of the MNA · RNA double helix is also seen in the deviation of some dihedral angles (*Table 6*) when compared with HNA · RNA or ANA · RNA: *e.g.*, α decreases from 282 (HNA) or 280° (ANA) to 269° in MNA. The torsion angle ε changes from 211 (HNA and ANA) to 222° (MNA). Also the RNA chain in the MNA · RNA helix has difficulties in maintaining an A-helix-like conformation. Thus, the average of torsion angle χ changes from 202° in A-RNA [38] to 213° in the RNA chain in MNA · RNA.

Moreover, the variability of torsion angles (see *Table 6*; *e.g.*, the standard deviation in α in the MNA chain is 19°, while it is 9° in the ANA chain) is higher in MNA · RNA than in ANA · RNA. The potential energy of the MNA · RNA system is also higher than that of the ANA · RNA system (*Fig. 4*). The minor-groove atoms in MNA become more accessible to the solvent (*Table 4*), and the minor groove becomes wider and shallower (*Fig. 8*), demonstrating a large deformation from a typical A-type helix. The deviation from the starting A-RNA conformation is shown in *Fig. 5,a*. It is clear that this deviation is more pronounced in the MNA · RNA duplex than it is in the ANA · RNA and HNA · RNA systems (which stay close to their starting conformations). A similar conformational change is also seen with single-stranded MNA. The energy of ssMNA is larger than the energy of ssANA (*Fig. 4,b*). Thus, ssMNA is potentially less stable than ssANA. In both ssMNA and MNA · RNA, the 3′-OH groups form intrastrand H-bonds to O–C(6′) of the following nucleotides (*Figs. 12* and *13*) unlike with ANA or ANA · RNA. This means that the origin of the instability of the MNA · RNA helix is the preferred H-bonding pattern involving the 3′-OH group.

Melting-temperature determinations reveal that the ANA · RNA duplex is more stable than the HNA · RNA duplex. This can be explained by several observations made during the present simulation studies. The SASA of the ANA · RNA duplex is more polar than the SASA of the HNA · RNA duplex due to the presence of the 3′-OH group in the former. This better hydration can lead to more stable associations due to the loss of highly structured H_2O molecules around the hydrophobic surface of the duplex. However, when the hydration of the single-stranded oligomer is taken into account, the difference in polarity of the SASA of ssHNA and HNA · RNA and of ssANA and ANA · RNA becomes small. This means that hydration cannot be the only factor underlying the difference in stability between HNA · RNA and ANA · RNA.

A second possible factor that may further explain the difference in stability between HNA · RNA and ANA · RNA is the difference in interstrand stacking between bases. However, as the sequences are the same and as there is no fundamental difference between the structure of HNA · RNA and ANA · RNA in modeling and NMR results, we do not believe that interstrand stacking will play a major role.

A third, apparently more important factor is the influence of single-strand preorganization on duplex stability (entropic benefit for hybridization). The ssANA is conformationally more restricted than ssHNA. The extra H-bonds between the 3′-OH groups and the O–C(4′) atoms in ssANA may have a stabilizing effect on the helical structure (mainly by stabilizing the torsion angle ε). Moreover, the O–C(3′) can be involved in enthalpic stabilization by H-bonding to the solvent H_2O (*Fig. 10*). The

conformational flexibility of the torsion angle ζ (*Fig. 14*) is more restricted in ANA than in HNA, due to the presence of the 3′-OH group. This group restricts the movement of the backbone for steric reasons. Finally, the ANA · RNA duplex is somewhat more compact than the HNA · RNA duplex (1.3 Å per 8 nucleotides). The compactness of the former duplex is similar to that of dsRNA. A more compact structure may result in a more favorable counter ion-nucleic acid interaction.

5. Conclusions. – In the present study, molecular dynamics was used to investigate the differences in duplex stability between HNA · RNA, ANA · RNA, and MNA · RNA. In MNA-containing complexes, the polar 3′-OH groups, which are poorly accessible to the solvent, form strong intrastrand H-bonds to the O–C(6′) of the following nucleotide. This not only restricts the conformation of MNA in its movements, but also slowly deforms and unwinds the A-RNA helical backbone structure. The more flexible RNA follows this deformed MNA conformation in the MNA · RNA duplex. In ANA-containing duplexes, the 3′-OH groups do not influence the general backbone conformation. There are no strong intrastrand H-bonds from the 3′-OH group to the following nucleotide. The higher stability of the ANA · RNA duplex when compared to the HNA · RNA duplex can be explained by *a*) a better hydration of the former duplex, *b*) the stabilization of the 3′-OH function of ANA by H-bonds to H_2O, *c*) the higher single-strand preorganization of ANA (when compared to ssHNA) mainly due to reduced conformational flexibility of torsion angles ζ (and ε), and *d*) a more favorable counter-ion effect due to the compactness of the structure. The substantial preorganization of the single-stranded hexitol-based nucleic acids HNA and ANA into the A-conformation of the double-helical nucleic acids (when compared to DNA and RNA) may give an explanation for their superior template characteristics in nonenzymatic oligomerization reactions.

The authors thank the *K. U. Leuven* (GOA 97/11) and *FWO* (GO11600) for financial support and are indebted to *Guy Schepers* and *Arthur Van Aerschot* for synthesizing the ANA sequence. We thank *Chantal Biernaux* for editorial help.

REFERENCES

[1] U. Essman, L. Perera, M. L. Berkowitz, T. Darden, H. Lee, L. G. Pedersen, *J. Chem. Phys.* **1995**, *103*, 8577.
[2] T. E. Cheatham III, J. L. Miller, T. Fox, T. A. Darden, P. A. Kollman, *J. Am. Chem. Soc*. **1995**, *117*, 4193.
[3] D. M. York, W. Yang, H. Lee, T. Darden, L. G. Pedersen, *J. Am. Chem. Soc.* **1995**, *117*, 5001.
[4] T. E. Cheatham III, P. A. Kollman, *J. Am. Chem. Soc.* **1997**, *119*, 4805.
[5] E. C. Sheler, S. A. Harris, R. Soliva, M. Orozco, C. A. Laughton, *J. Am. Chem. Soc.* **1999**, *121*, 5981.
[6] H. De Winter, E. Lescrinier, A. Van Aerschot, P. Herdewijn, *J. Am. Chem. Soc.* **1998**, *120*, 5381.
[7] A. Van Aerschot, I. Verheggen, C. Hendrix, P. Herdewijn, *Angew. Chem., Int. Ed.* **1995**, *34*, 1338.
[8] C. Hendrix, H. Rosemeyer, I. Verheggen, F. Seela, A. Van Aerschot, P. Herdewijn, *Chem. – Eur. J.* **1997**, *3*, 110.
[9] C. Hendrix, H. Rosemeyer, B. De Bouvere, A. Van Aerschot, F. Seela, P. Herdewijn, *Chem. – Eur. J.* **1997**, *3*, 1513.
[10] I. Kozlov, P. Politis, A. Van Aerschot, R. Busson, P. Herdewijn, L. Orgel, *J. Am. Chem. Soc.* **1999**, *121*, 2653.
[11] I. Kozlov, B. De Bouvere, A. Van Aerschot, P. Herdewijn, L. Orgel, *J. Am. Chem. Soc.* **1999**, *121*, 5856.
[12] I. Kozlov, P. Politis, S. Pitsch, P. Herdewijn, L. Orgel, *J. Am. Chem. Soc.* **1999**, *121*, 1108.
[13] N. Hossain, B. Wroblowski, A. Van Aerschot, J. Rozenski, A. De Bruyn, P. Herdewijn, *J. Org. Chem.* **1998**, *63*, 1574.
[14] B. Allart, K. Khan, H. Rosemeyer, G. Schepers, C. Hendrix, K. Rothenbacher, F. Seela, A. Van Aerschot, P. Herdewijn, *Chem. – Eur. J.* **1999**, *5*, 2424.

[15] P. Herdewijn, B. Allart, B. De Bouvere, H. De Winter, C. Hendrix, N. Hossain, G. Schepers, I. Verheggen, B. Wroblowski, A. Van Aerschot, *Nucleosides Nucleotides* **1999**, *18*, 1371.
[16] W. D. Cornell, P. Cieplak, C. I. Bayly, I. R. Gould, K. M. Merz Jr., D. M. Ferguson, D. C. Spellmeyer, T. Fox, J. W. Caldwell, P. A. Kollman, *J. Am. Chem. Soc.* **1995**, *117*, 5179.
[17] C. I. Bayly, P. Cieplak, W. D. Cornell, P. A. Kollman, *J. Phys. Chem*. **1993**, *97*, 10269.
[18] M. W. Schmidt, K. K. Baldridge, J. A. Boatz, S. T. Elbert, G. S. Gordon, J. H. Jensen, S. Koseki, N. Matsunaga, K. A. Nguyen, S. Su, T. L. Windus, M. Dupuis, J. A. Montgomery, *J. Comput. Chem.* **1993**, *14*, 1347.
[19] R. A. Sayle, E. J. Milner-White, *Trends Biochem. Sci*. **1995**, *20*, 374.
[20] T. E. Ferrin, C. C. Huang, L. E. Jarvis, R. Langridge, *J. Mol. Graphics* **1988**, *6*, 13, 36.
[21] S. Arnott, D. W. L. Hukins, *Biochem. Biophys. Res. Commun.* **1972**, *47*, 1504.
[22] W. Jorgensen, J. Chandrasekar, J. Madura, R. Impey, M. Klein, *J. Chem. Phys.* **1983**, *79*, 926.
[23] H. J. C. Berendsen, J. P. M. Postma, W. F. van Gunsteren, A. DiNola, J. R. Haak, *J. Comput. Phys.* **1984**, *81*, 3684.
[24] W. F. van Gunsteren, H. J. C. Berendsen, *Mol. Phys.* **1977**, *5*, 1311.
[25] D. Cremer, J. A. Pople, *J. Am. Chem. Soc*. **1975**, *97*, 1354.
[26] C. Altona, M. Sundaralingam, *J. Am. Chem. Soc.* **1972**, *94*, 8205.
[27] F. M. Richards, *Annu. Rev. Biophys. Bioeng*. **1977**, *6*, 151.
[28] R. Lavery, H. Sklenar, *J. Biomol. Struct. Dynam.* **1988**, *6*, 63.
[29] B. De Bouvere, L. Kerremans, J. Rozenski, G. Janssen, A. Van Aerschot, P. Claes, R. Busson, P. Herdewijn, *Liebigs Ann. Chem*. **1997**, 1453.
[30] B. Allart, R. Busson, J. Rozenski, A. Van Aerschot, P. Herdewijn, *Tetrahedron* **1999**, *55*, 6527.
[31] D. J. States, R. A. Haberkorn, D. J. Ruben, *J. Magn. Reson*. **1982**, *48*, 286.
[32] P. Plateau, M. Guéron, *J. Am. Chem. Soc.* **1982**, *104*, 7310.
[33] J. Jeener, B. H. Meier, P. Bachman, R. R. Ernst, *J. Chem. Phys.* **1979**, *71*, 4546.
[34] V. Sklenar, H. Miyashiro, G. Zon, H. T. Miles, A. Bax, *FEBS Letters* **1986**, *208*, 94.
[35] W. Kauzmann, *Adv. Protein Chem.* **1959**, *14*, 1.
[36] D. Sitkoff, K. A. Sharp, B. J. Honig, *Phys. Chem*. **1994**, *98*, 1978.
[37] C. L. Brooks III, M. Karplus, B. M. Pettitt, 'Proteins, a Theoretical Perspective of Dynamics, Structure and Thermodynamics', Wiley, New York, 1988.
[38] W. Saenger, 'Principles of Nucleic Acid Structure', Springer-Verlag, New York, 1984.
[39] N. Yathindra, M. Sundaralingam, *Proc. Natl. Acad. Sci. U.S.A*. **1974**, *71*, 3325.
[40] E. Lescrinier, J. Schraml, R. Busson, H. Heus, C. Hilbers, P. Herdewijn, *Chem. Biol.* **2000**, in press.
[41] J. N. S. Evans, 'Biomolecular NMR Spectroscopy', Oxford University Press, 1995, 343.
[42] K. Wütrich, 'NMR of Proteins and Nucleic Acids', 1986, New York, Wiley, p. 218.
[43] D. G. Gorenstein, *Methods Enzymol.* **1992**, *211*, 254.
[44] M. Vandermeeren, S. Preveral, S. Janssens, J. Geysen, E. Saison-Behmoaras, A. Van Aerschot, P. Herdewijn, *Biochem. Pharmacol*. **2000**, *59*, 655.
[45] A. Eschenmoser, M. Dobler, *Helv. Chim. Acta* **1992**, *75*, 218.
[46] P. J. Kraulis, *J. Appl. Crystallogr.* **1991**, *24*, 946.
[47] R. M. Esnouf, *J. Mol. Graphics* **1997**, *15*, 132.
[48] P. J. Turner, 'xmgr ace/gr 3.01', 1994.
[49] K. K. H. Toh, 'Plotmtv 1.4.1', 1995.

Received May 19, 2000